UNIVERSITY OF ZAGREB
**FACULTY OF ELECTRICAL ENGINEERING AND COMPUTING**

Master thesis no. 1822

# Switch-mode radiofrequency amplifiers with complementary filters

Ante Brizić

Zagreb, June 2019

*Umjesto ove stranice umetnite izvornik Vašeg rada.*
*Da bi ste uklonili ovu stranicu obrišite naredbu* `\izvornik`.

# Contents

**List of Figures** **vi**

**List of Tables** **viii**

**1. Introduction** **1**

**2. Filter design** **3**

2.1. Introduction . . . . . 3

2.2. Topology . . . . . 3

2.3. Design conditions . . . . . 4

2.3.1. First order . . . . . 5

2.3.2. Second order . . . . . 5

2.3.3. Third order . . . . . 6

2.3.4. Fourth order . . . . . 6

2.4. Filter assembly and measurements . . . . . 8

2.4.1. 800 MHz filters . . . . . 9

2.4.2. 2.5 GHz filters . . . . . 14

2.5. Filter design conclusion . . . . . 17

**3. Drain efficiency of an SMPA terminated with a complementary filter** **18**

3.1. Introduction . . . . . 18

3.2. Drain efficiency . . . . . 18

3.3. Experimental verification . . . . . 22

3.4. Drain efficiency is greater when terminated /w complementary filter 24

3.5. Drain efficiency is more stable when terminated /w complementary filter . . . . . 26

3.6. Conclusions on drain efficiency . . . . . 29

**4. Time-domain reflectometry as a quality test** **30**
4.1. Introduction . . . . . 30
4.2. TDR fundamentals . . . . . 30
4.3. Measuring the filters . . . . . 31
4.4. TDR simulation program using MATLAB . . . . . 34
4.5. Simulation of the complementary filter TDR response . . . . . 35
4.6. TDR conclusion . . . . . 37

**5. Conclusion** **38**
5.1. Acknowledgment . . . . . 39

**Bibliography** **40**

# List of Figures


2.1. Two possible architectures of a complementary two-way diplexer filter: ($a$) admittance complementary and ($b$) impedance complementary filters. . . . . 3

2.2. Circuit diagrams for first four orders of complementary ladder filters examined in this work: the circuit diagrams ($a$) through ($d$) correspond to the first to fourth order filters. The port designations are shown in circled numbers. . . . . 4

2.3. Transfer functions for Butterworth filter sections . . . . . 7

2.4. Smith diagram of the diplexers input impedances, note the direction of increasing frequency with the arrow: $''f''$ . . . . . 8

2.5. Crosssection of the Rogers 4350B PCB substrate . . . . . 8

2.6. ($a$) Printed circuit board design and ($b$) fourth-order 2.5 GHz filter assembled with 0402 inductors and 0603 capacitors. . . . . 9

2.7. ($a$) ADS simulation ($b$) VNA measurements c) PCB filter sample for the first order 800 MHz complementary diplexer . . . . . 11

2.8. ($a$) ADS simulation ($b$) VNA measurements c) PCB filter sample for the second order 800 MHz complementary diplexer . . . . . 11

2.9. ($a$) ADS simulation ($b$) VNA measurements c) PCB filter sample for the third order 800 MHz complementary diplexer . . . . . 12

2.10. ($a$) ADS simulation ($b$) VNA measurements c) PCB filter sample for the fourth order 800 MHz complementary diplexer . . . . . 12

2.11. ($a$) ADS simulation ($b$) VNA measurements PCB filter sample for the first order 2.5 GHz complementary diplexer . . . . . 15

2.12. ($a$) ADS simulation ($b$) VNA measurements PCB filter sample for for the second order 2.5 GHz complementary diplexer . . . . . 15

2.13. ($a$) ADS simulation ($b$) VNA measurements PCB filter sample for the third order 2.5 GHz complementary diplexer . . . . . 16

2.14. ($a$) ADS simulation ($b$) VNA measurements PCB filter sample for the fourth order 2.5 GHz complementary diplexer . . . . . 16

3.1. Lossless low-pass filter on the output of an SMPA . . . . . 19
3.2. Lossless low-pass filter scattering parameters characteristic . . . . 19
3.3. Lossless all-pass filter on the output of an SMPA . . . . . 20
3.4. All-pass filter scattering parameters characteristic . . . . . 21
3.5. Lossless all-pass filter on the output of an SMPA . . . . . 22
3.6. Filter termination experiment . . . . . 22
3.7. $Z_0$ termination experiment . . . . . 23
3.8. Measurement setup . . . . . 24
3.9. Output waveform capture with a digitizing signal oscilloscope (DSO) 25
3.10. Output waveforms on 540 MHz for a loseless LP and input $Z_0$ loseless LP filter . . . . . 25
3.11. Output waveforms on 540 MHz for a lossless complementary diplexer and input $Z_0$ diplexer filter . . . . . 26
3.12. Output waveform on 1260 MHz for a LLLP and input $Z_0$ LLLP filter . . . . . 28
3.13. Output waveform on 1260 MHz for a lossless complementary diplexer and input $Z_0$ diplexer filter . . . . . 29

4.1. TDR response for various termination and discontinuities . . . . . 31
4.2. TDR response for various termination and discontinuities . . . . . 31
4.3. TDR response for various termination and discontinuities . . . . . 31
4.4. TDR response for various termination and discontinuities . . . . . 32
4.5. Schematic of the two tested filters . . . . . 32
4.6. TDR waveforms of the LLLP and complementary filter . . . . . 33
4.7. Closeup TDR waveforms complementary filter showing the *parasitic* discontinuities . . . . . 33
4.8. Complementary filter $s$ parameters with delay lines in one of the branches . . . . . 34
4.9. TDR program flowchart . . . . . 35
4.10. TDR simulation of a series inductor discontinuity network . . . . 36
4.11. TDR simulation of the complementary filter response (black) and measured complementary filter response (red dashed) . . . . . 36

# List of Tables

2.1. Element values for the 800 MHz diplexer . . . . . 10
2.2. Element values for the 2.5 GHz diplexer . . . . . 14

3.1. Measured parameters on 540 MHz . . . . . 24
3.2. Measured parameters on 1260 MHz . . . . . 27

# 1. Introduction

This masters thesis introduces and experimentally demonstrates a new approach to stabilizing and improving the efficiency of switchmode radiofrequency (RF) amplifiers by using constant-resistance filters at their output. As switchmode RF amplifiers always require some degree of harmonic filtering, the successful demonstration of these beneficial effects opens a new application for constant-resistance filters.

Constant-resistance filters are a class of absorptive filters that ideally present no reflection to an RF signal of any frequency incident from a transmission line with constant characteristic impedance, while their transfer function can be designed to exhibit low-pass, high-pass, or band-pass characteristics. This type of filter has been investigated for a variety of applications for almost a century [1], [2], [3] and has been widely used to control the frequency response of transmission lines and amplifiers in communications systems [4], [5] and phase distortion and speaker impedance responses in audio systems.

Constant-resistance filters are also referred to as reflectionless filters in the industry. They can be asymmetric in that zero reflection is available only on one port or symmetric in which both ports exhibit zero reflection. A number of network synthesis approaches have been developed for the asymmetric design over the years [6], [5], [7], [8], [9], [10], while the progress in symmetric reflectionless filters has been more recent [11], [12]. In this work, we investigate diplexer-type absorbing low-pass filters, which are a subset of constant-resistance filters with asymmetric circuit configuration. In a diplexer reflectionless low-pass filter, the filter comprises two filters: one exhibiting the desired low-pass transmission characteristic and its low-pass output terminal, and one exhibiting high-pass characteristics and associated high-pass output terminal. The constant resistance networks in this work hence contain exclusively two filters, a low-pass and high-pass network that are connected in parallel at the input terminal so that the input impedance of the entire network is $Z_0$.

In order to achieve zero reflection at all frequencies from the input terminal, the designs of these two filters are mutually dependent on each other and we refer to such filter pairs as *complementary* filters.

The novelty in this work lies in using complementary reflectionless filters at the output of a radiofrequency switchmode power amplifier (RF-SMPA) in order to increase its drain efficiency. The SMPAs are progressively more commonly used in mobile phones and base stations today and the increase in the efficiency is beneficial to their commercialization (for example, less heating in mobile phones prolongs the battery life). Furthermore, to the best of knowledge there are no reports in which reflectionless filters are used for this purpose in conjunction with RF-SMPAs.

The work presented here consists of the design, simulations, assembly and measurements of the filters connected to the output of an SMPA. Design conditions and parameters are given while the measurements are shown in their corresponding tables. Both the theory and our measurements support the conclusion that the SMPA terminated with complementary filters exhibits higher and more consistent efficiency than when terminated with a standard lossless low-pass filter.

# 2. Filter design

## 2.1. Introduction

This chapter covers the principles and design methods for the assembly of complementary filters in a diplexer architecture. A filter topology has been presented, simulated, assembled and measured. The simulations have been compared to the measurements and the measured filters were evaluated for the use with switch-mode amplifiers (SMPAs).

## 2.2. Topology

There are two common realizations of complementary filters that consist of a single low-pass and high-pass filter. They are shown on figure 2.1, where $(a)$ denotes the *admittance complementary* diplexer filter in which the low-pass and the high-pass filter are connected in parallel, while $(b)$ presents the *impedance complementary* diplexer filter where the low-pass and high-pass sections are connected in series.

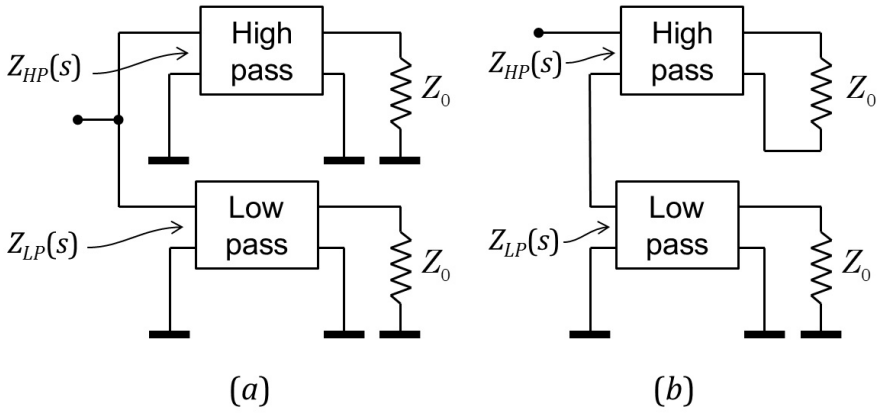


**Figure 2.1:** Two possible architectures of a complementary two-way diplexer filter: $(a)$ admittance complementary and $(b)$ impedance complementary filters.

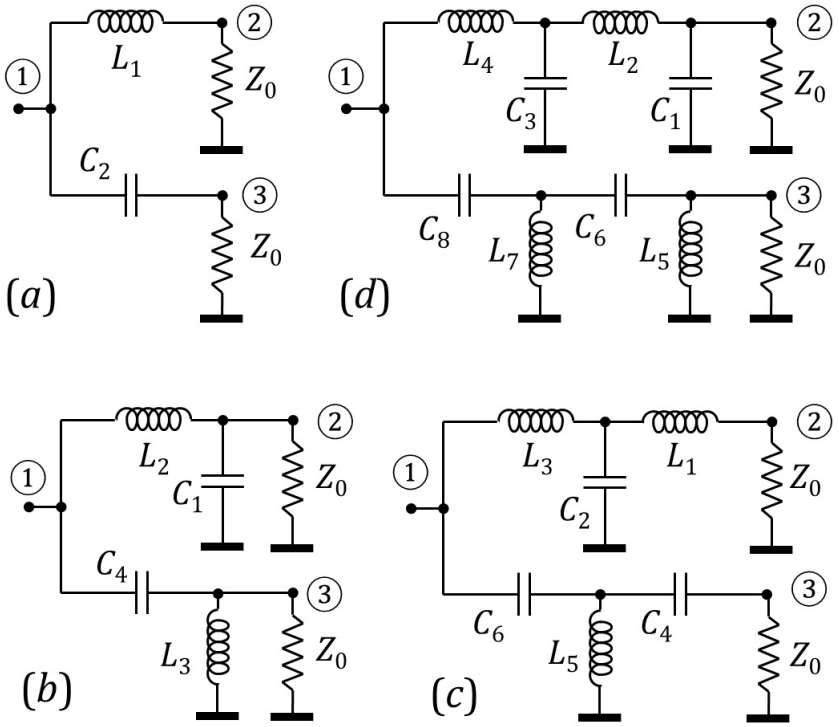


**Figure 2.2:** Circuit diagrams for first four orders of complementary ladder filters examined in this work: the circuit diagrams ($a$) through ($d$) correspond to the first to fourth order filters. The port designations are shown in circled numbers.

We chose to use the *admittance complementary* diplexer filter as shown on figure 2.1 ($a$) due to the fact that the coupling to the high-pass section is significantly simpler. Furthermore we decided to implement both the low-pass and high-pass sections as lossless ladder filters. The first four orders of such diplexer networks are shown on figure 2.2. The transfer function through the low-pass section (port 1 to port 2) when terminated with $Z_0$ has a low-pass characteristic and the transfer function through the high-pass section (port 1 to port 3) has a high-pass filter characteristic.

## 2.3. Design conditions

In order to achieve the minimal reflection on the input for the networks shown in figure 2.2 the impedance of the low-pass $Z_{LP}(s)$ and high-pass $Z_{HP}(s)$ network have to satisfy the identity:

$$\frac{1}{Z_{LP}(s)} + \frac{1}{Z_{HP}(s)} = \frac{1}{Z_0} \tag{2.1}$$

where $Z_0$ is the characteristics impedance of the transmission lines in the system and $\mathrm{Im}(Z_0) = 0$.

Each filter is characterized with the crossover frequency ($\omega_0$) as the frequency at which the power transfer function of the low-pass section $|s_{21}(\omega_0)|^2$ and the high-pass section $|s_{31}(\omega_0)|^2$ equal each equal to 1/2.

### 2.3.1. First order

The first order complementary filter, shown in Figure 2.2($a$), will exhibit input impedance equal to $Z_0$ if $C_2 Z_0^2 = L_1$. The $L_1$ and $C_2$ are related through the crossover frequency $\omega_0$. It is straightforward to show that the component values that satisfy equation 2.1 are:

$$L_1 = \frac{Z_0}{\omega_0} \qquad\qquad C_2 = \frac{1}{\omega_0 Z_0} \tag{2.2}$$

The transfer functions at the output on ports 2 and 3 are respectively:

$$s_{21}(s) = \frac{1}{s/\omega_0 + 1} \qquad\qquad s_{31}(s) = \frac{s/\omega_0}{1 + s/\omega_0} \tag{2.3}$$

### 2.3.2. Second order

The second order complementary filter, shown in figure 2.2($b$), will exhibit input impedance equal to $Z_0$ if $C_1 = C_4 = C$ , $L_1 = L_3 = C$ and $2L = CZ_0^2$. The $C$ and $L$ are again related through the crossover frequency $\omega_0$. We can show that the component values that satisfy equation 2.1 are:

$$L_3 = L_2 = \sqrt{2}\left(\frac{Z_0}{\omega_0}\right) \qquad\qquad C_1 = C_4 = \frac{1}{\sqrt{2}} \cdot \frac{1}{\omega_0 Z_0} \tag{2.4}$$

The transfer functions follows:

$$s_{21}(s) = \frac{1}{\left(\frac{s}{\omega_0}\right)^2 + \sqrt{2}\left(\frac{s}{\omega_0}\right) + 1} \tag{2.5}$$

$$s_{31}(s) = \frac{\left(\frac{s}{\omega_0}\right)^2}{\left(\frac{s}{\omega_0}\right)^2 + \sqrt{2}\left(\frac{s}{\omega_0}\right) + 1} \tag{2.6}$$

### 2.3.3. Third order

The third order complementary filter, as shown in figure 2.2($c$) will be $Z_0$ resistive for the next derived component values (while satisfying equation 2.1):

$$L_1 = \frac{1}{2}\left(\frac{Z_0}{\omega_0}\right) \qquad C_2 = \frac{4}{3}\cdot\frac{1}{Z_0\omega_0} \tag{2.7}$$

$$L_3 = \frac{3}{2}\left(\frac{Z_0}{\omega_0}\right) \qquad C_4 = 2\cdot\frac{1}{Z_0\omega_0} \tag{2.8}$$

$$L_5 = \frac{3}{4}\left(\frac{Z_0}{\omega_0}\right) \qquad C_6 = \frac{2}{3}\cdot\frac{1}{Z_0\omega_0} \tag{2.9}$$

The transfer functions on the ports 2 and 3 are:

$$s_{21}(s) = \frac{1}{\left(\frac{s}{\omega_0}\right)^3 + 2\left(\frac{s}{\omega_0}\right)^2 + 2\left(\frac{s}{\omega_0}\right) + 1} \tag{2.10}$$

$$s_{31}(s) = \frac{\left(\frac{s}{\omega_0}\right)^3}{\left(\frac{s}{\omega_0}\right)^3 + 2\left(\frac{s}{\omega_0}\right)^2 + 2\left(\frac{s}{\omega_0}\right) + 1} \tag{2.11}$$

### 2.3.4. Fourth order

The fourth order complementary filter, as shown in figure 2.2($d$) will be $Z_0$ resistive for the next derived component values (while satisfying equation 2.1):

$$\alpha = 2\sqrt{\frac{2+\sqrt{2}}{2}} \qquad \beta = 2+\sqrt{2} \tag{2.12}$$

$$L_2 = \frac{\alpha}{\beta-1}\left(\frac{Z_0}{\omega_0}\right) \qquad C_1 = \frac{1}{\alpha}\cdot\frac{1}{Z_0\omega_0} \tag{2.13}$$

$$L_4 = \frac{\alpha(\beta-2)}{\beta-1}\left(\frac{Z_0}{\omega_0}\right) \qquad C_3 = \frac{1}{\alpha}\frac{(\beta-1)^2}{\beta-2}\cdot\frac{1}{Z_0\omega_0} \tag{2.14}$$

$$L_5 = \alpha\left(\frac{Z_0}{\omega_0}\right) \qquad C_6 = \frac{\beta-1}{\alpha}\cdot\frac{1}{Z_0\omega_0} \tag{2.15}$$

$$L_7 = \alpha\frac{\beta-2}{(\beta-1)^2}\left(\frac{Z_0}{\omega_0}\right) \qquad C_8 = \frac{\beta-1}{\alpha(\beta-2)}\cdot\frac{1}{Z_0\omega_0} \tag{2.16}$$

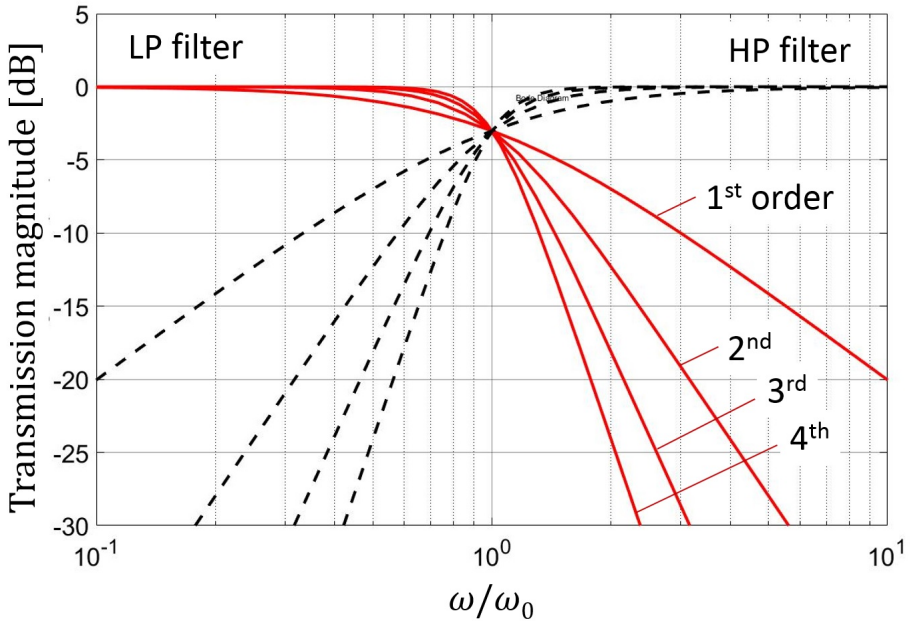


**Figure 2.3:** Transfer functions for Butterworth filter sections

The transfer functions:

$$s_{21}(s) = \frac{1}{\left(\frac{s}{\omega_0}\right)^4 + \alpha\left(\frac{s}{\omega_0}\right)^3 + \beta\left(\frac{s}{\omega_0}\right)^2 + \alpha\left(\frac{s}{\omega_0}\right) + 1} \tag{2.17}$$

$$s_{31}(s) = \frac{\left(\frac{s}{\omega_0}\right)^4}{\left(\frac{s}{\omega_0}\right)^4 + \alpha\left(\frac{s}{\omega_0}\right)^3 + \beta\left(\frac{s}{\omega_0}\right)^2 + \alpha\left(\frac{s}{\omega_0}\right) + 1} \tag{2.18}$$

**As the reader may notice, the transfer functions are actually all Butterworth types.** In fact, if we require that the low-pass and the high-pass filters be ladder-filters with a single component in each ladder position, then the only solution for admittance-complementary filter is that both the low-pass and the high-pass sections be Butterworth filters.

Figure 2.3 illustrates the transfer functions of the low-pass $|s_{21}(\omega/\omega_0)|^2$ section and the high-pass $|s_{31}(\omega/\omega_0)|^2$ sections for first four Butterworth orders. Similarly, Figure 2.4 shows the corresponding Smith diagrams.

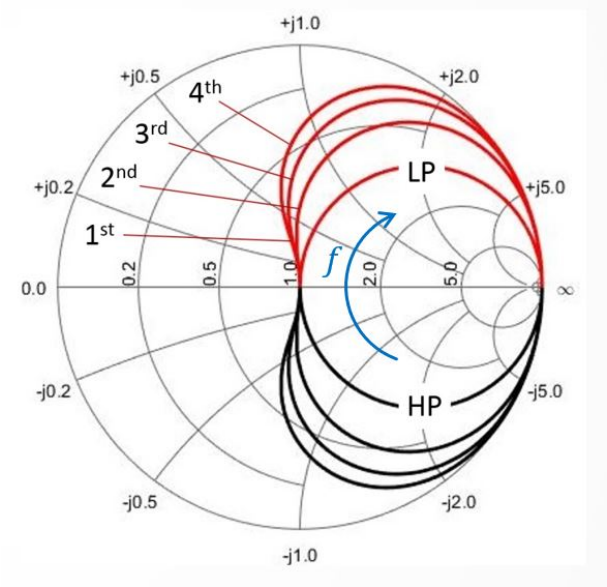


**Figure 2.4:** Smith diagram of the diplexers input impedances, note the direction of increasing frequency with the arrow: *"f"*

## 2.4. Filter assembly and measurements

All four filter designs were assembled with the purpose of investigating performance and implementation. A set of four filters with a crossover frequency on 800 MHz and another four on 2500 MHz have been assembled. First we simulated the filters performance and aftermath they were assembled on a printed circuit board with discrete components with a 10% tolerance as shown in figure 2.6($a$). The printed circuit board features one input transmission line in the middle of the board allowing the implementation of the two filter networks.The printed circuit board substrate material was Rogers 4350B[13] and the substrate thickness was 0.5 mm (20 mils). The crosssection of the substrate is shown in figure 2.5.

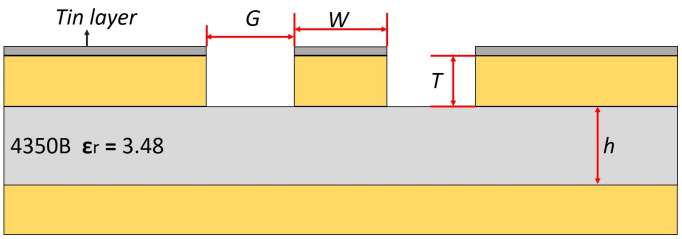


**Figure 2.5:** Crosssection of the Rogers 4350B PCB substrate

Surface-mountable 0603 thin-film capacitors and 0402 wirewound inductors were used, while ground-backed coplanar waveguide was used for transmission

lines. The boards were connectorized using bolt-on end-launch SMA connectors [14]. An implementation of such a filter is shown on figure 2.6($b$).

The filters were characterized using $s$-parameter measurements performed on a 40-GHz vector network analyzer (VNA). We were primarily interested in the magnitude of the reflection coefficient $|s_{11}|^2$, for which we used open-short-load single-port calibration on the VNA, and the transmission properties of both branches of the filter $|s_{21}|^2$ and $|s_{31}|^2$, for which we added two 10-dB attenuators at the VNA ports and calibrated by normalizing the transmission through the attenuated path. The attenuators are needed to eliminate the reflection from the VNA ports and they enable significantly simpler and quicker calibration procedure.

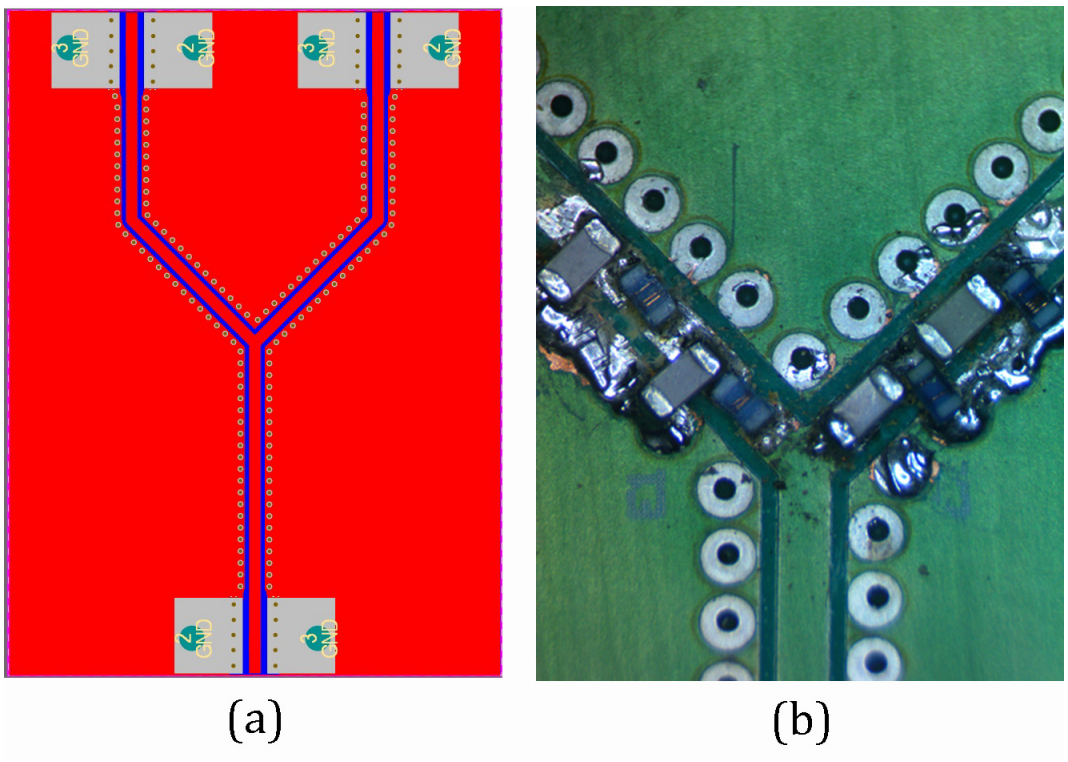


**Figure 2.6:** ($a$) Printed circuit board design and ($b$) fourth-order 2.5 GHz filter assembled with 0402 inductors and 0603 capacitors.

### 2.4.1. 800 MHz filters

The filter element values computed with the equations from section 2.3 are shown in table 2.1.

| Order | Inductance by design [nH] | Inductance taken [nH] | Capacitance by design [pF] | Capacitance taken [pF] |
|---|---|---|---|---|
| 1. | $L_1 = 9.95$ | 10 | $C_2 = 3.979$ | 4 |
| 2. | $L_2 = 14.07$ | 15 | $C_1 = 2.814$ | 2.7 |
| | $L_3 = 14.07$ | 15 | $C_4 = 2.814$ | 2.7 |
| 3. | $L_1 = 4.97$ | 5 | $C_2 = 5.305$ | 4 |
| | $L_3 = 14.92$ | 15 | $C_4 = 7.958$ | 8 |
| | $L_5 = 7.46$ | 7.5 | $C_6 = 2.653$ | 2.7 |
| 4. | $L_1 = 10.77$ | 11 | $C_2 = 1.52$ | 1.5 |
| | $L_3 = 15.23$ | 15 | $C_4 = 6.28$ | 6.3 |
| | $L_5 = 25.99$ | 27 | $C_6 = 3.68$ | 3.6 |
| | $L_5 = 6.31$ | 6.3 | $C_6 = 2.59$ | 2.6 |

**Table 2.1:** Element values for the 800 MHz diplexer

On figures 2.7, 2.8, 2.9 and 2.10 in part *(a)* we show the ADS simulation of the 800 MHZ filters while on part *(b)* we show the VNA measurements of the $s_{11}$(red), $s_{21}$ (black) and $s_{31}$ (black dashed). On the simulations we show that there exists a local maxima at 800 MHz on $s_{11}$, however before and after, it falls back under 50 dB. On the measurements we show that the local maxima still exists, however the filters fall off on higher frequencies due to the parasitic elements of the used lumped components [15].

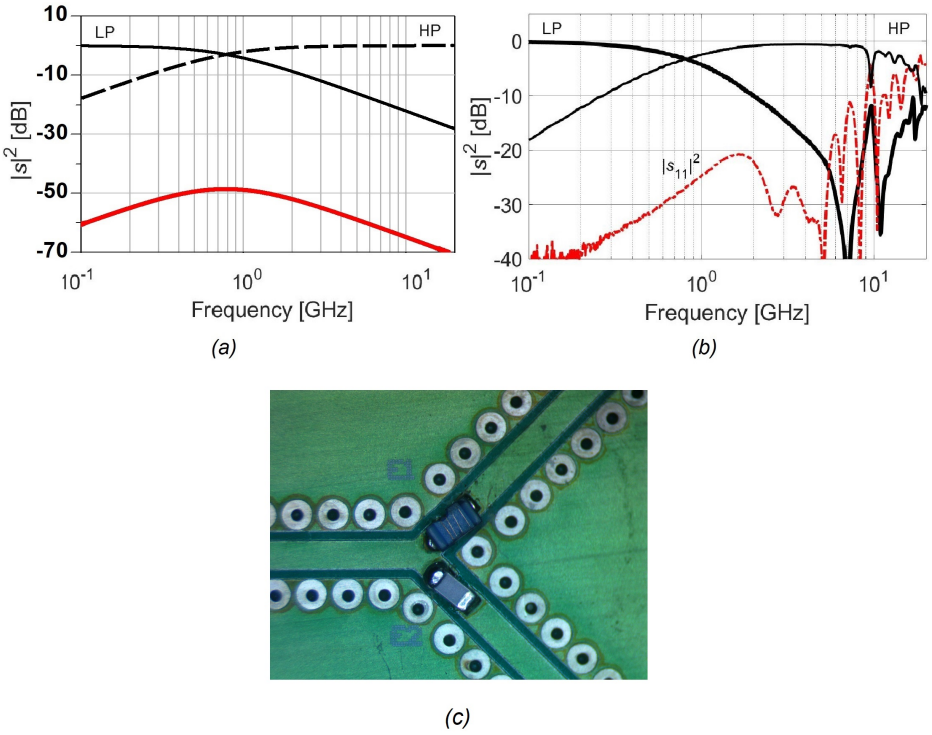


**Figure 2.7:** ($a$) ADS simulation ($b$) VNA measurements c) PCB filter sample for the first order 800 MHz complementary diplexer

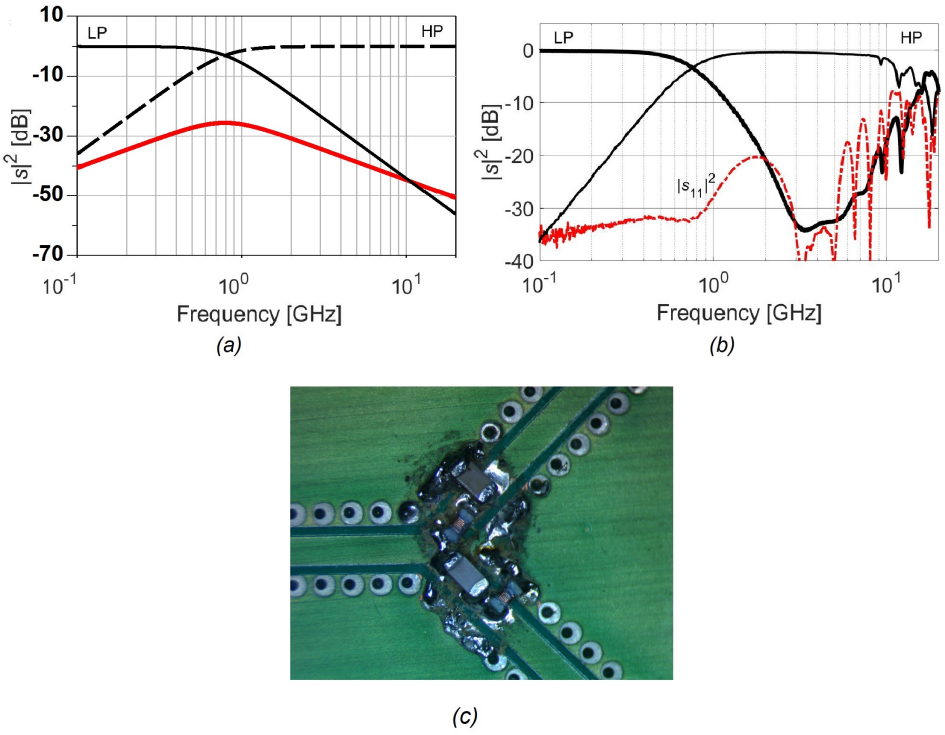


**Figure 2.8:** ($a$) ADS simulation ($b$) VNA measurements c) PCB filter sample for the second order 800 MHz complementary diplexer

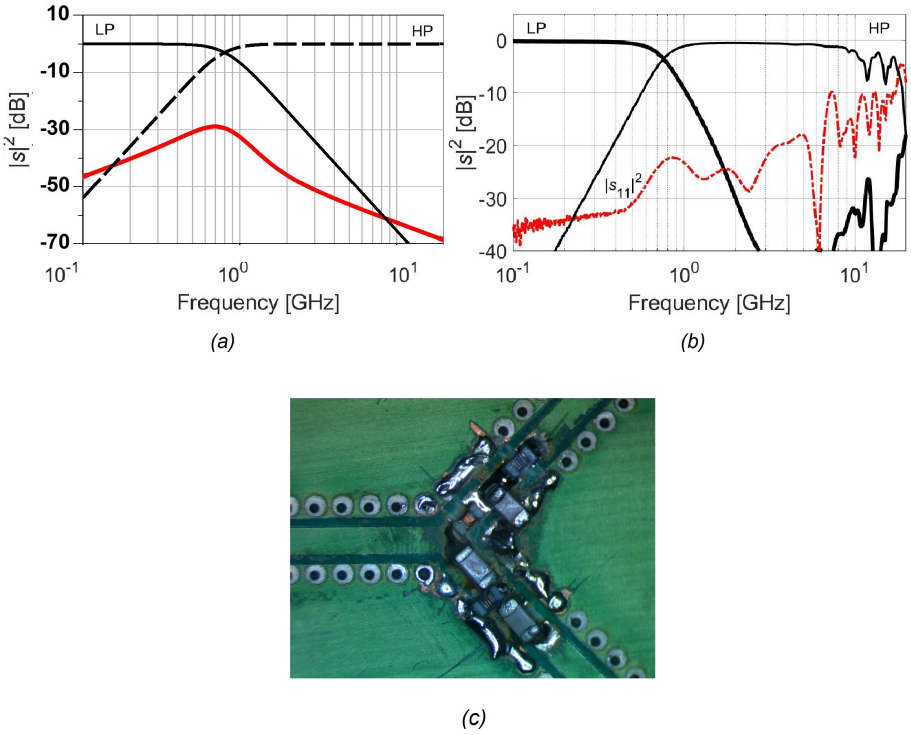


**Figure 2.9:** $(a)$ ADS simulation $(b)$ VNA measurements c) PCB filter sample for the third order 800 MHz complementary diplexer

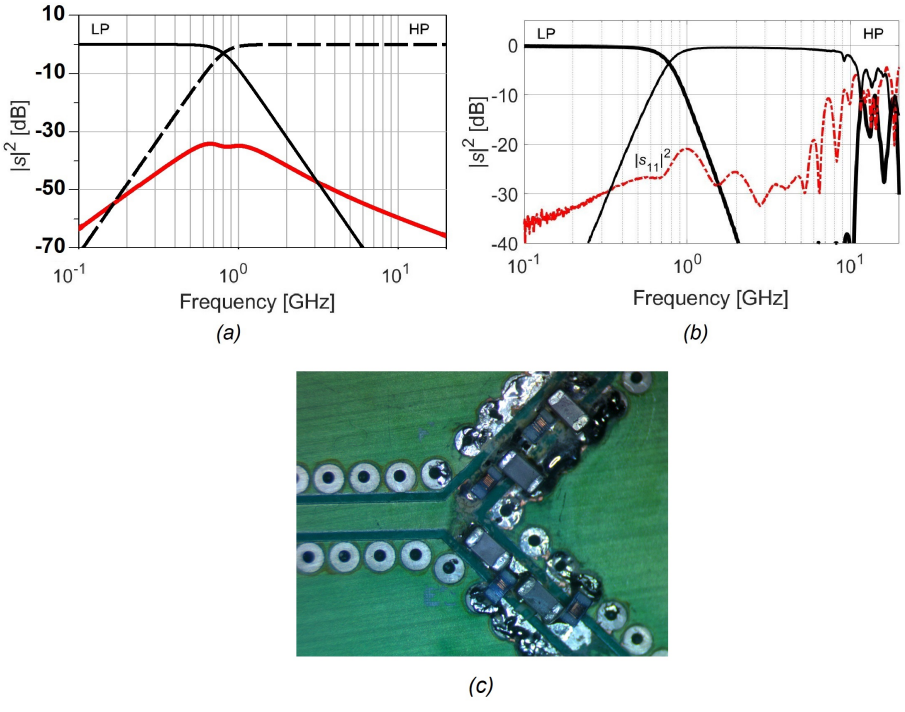


**Figure 2.10:** $(a)$ ADS simulation $(b)$ VNA measurements c) PCB filter sample for the fourth order 800 MHz complementary diplexer

**We consider -20dB reflection acceptable for use in our complementary filters. Under this conditions the filters are usable up to 4-5GHz depending on the order. For that frequency $s_{11}$ is less than 20dB. Therefore for fundamental frequencies up to 800MHz these filters can be used to properly terminate 9 or 10 harmonics.**

### 2.4.2. 2.5 GHz filters

The filter element values computed with the equations from section 2.3 are shown in table 2.2. Again, all components have up to 10% tolerance and are wire-wound 0402 inductances and 0603 thin film capacitors. For all of the elements ADS simulations and VNA measurements have been made and they are shown on figures 2.11, 2.12, 2.13 and 2.14.

| Order | Inductance by design [nH] | Inductance taken [nH] | Capacitance by design [pF] | Capacitance taken [pF] |
|---|---|---|---|---|
| 1. | $L_1 = 3.18$ | 3.3 | $C_2 = 1.27$ | 1.2 |
| 2. | $L_2 = 4.50$ | 4.3 | $C_1 = 0.90$ | 0.9 |
| | $L_3 = 4.50$ | 4.3 | $C_4 = 0.90$ | 0.9 |
| 3. | $L_1 = 1.59$ | 1.8 | $C_2 = 1.69$ | 1.8 |
| | $L_3 = 4.78$ | 4.7 | $C_4 = 2.55$ | 2.7 |
| | $L_5 = 2.39$ | 2.2 | $C_6 = 0.85$ | 0.9 |
| 4. | $L_1 = 3.45$ | 3.6 | $C_2 = 0.49$ | 0.5 |
| | $L_3 = 4.87$ | 4.7 | $C_4 = 2.01$ | 2 |
| | $L_5 = 8.32$ | 8.2 | $C_6 = 1.18$ | 1.2 |
| | $L_5 = 2.02$ | 2 | $C_6 = 0.83$ | 0.8 |

**Table 2.2:** Element values for the 2.5 GHz diplexer

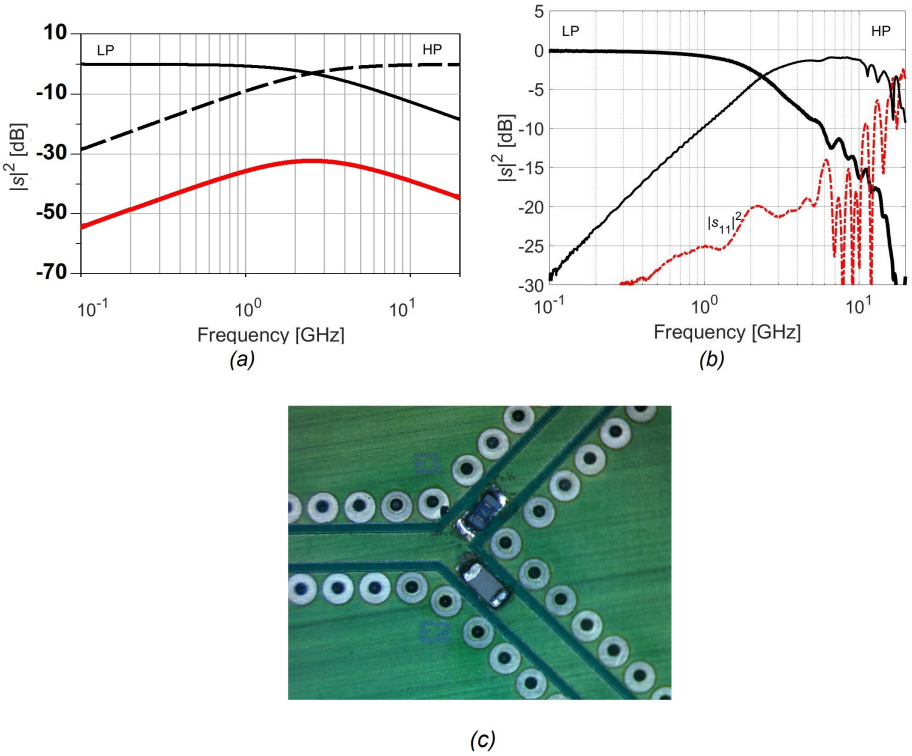


**Figure 2.11:** $(a)$ ADS simulation $(b)$ VNA measurements PCB filter sample for the first order 2.5 GHz complementary diplexer

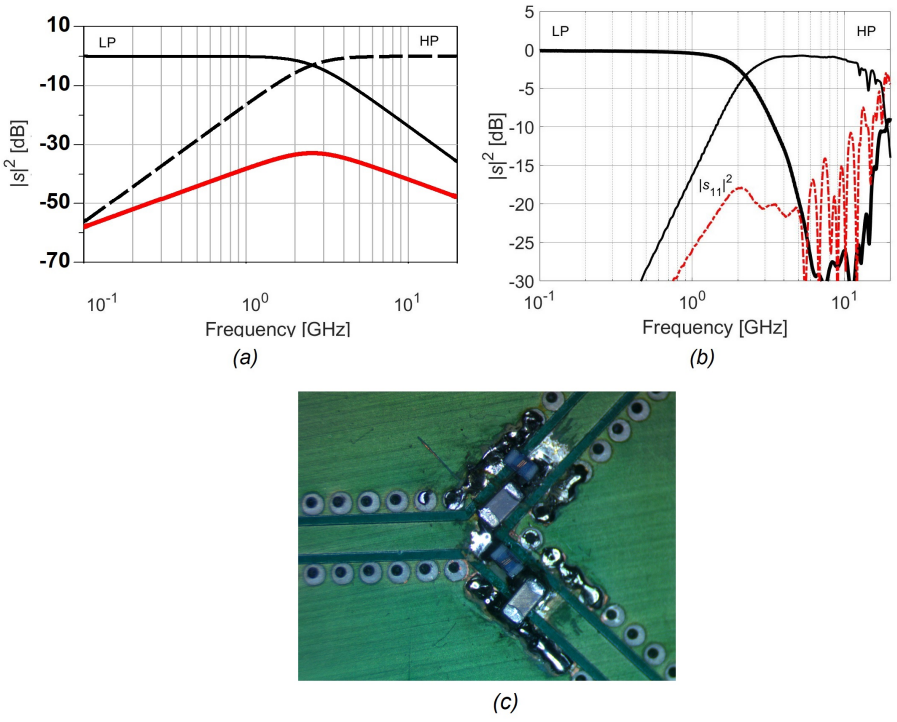


**Figure 2.12:** $(a)$ ADS simulation $(b)$ VNA measurements PCB filter sample for for the second order 2.5 GHz complementary diplexer

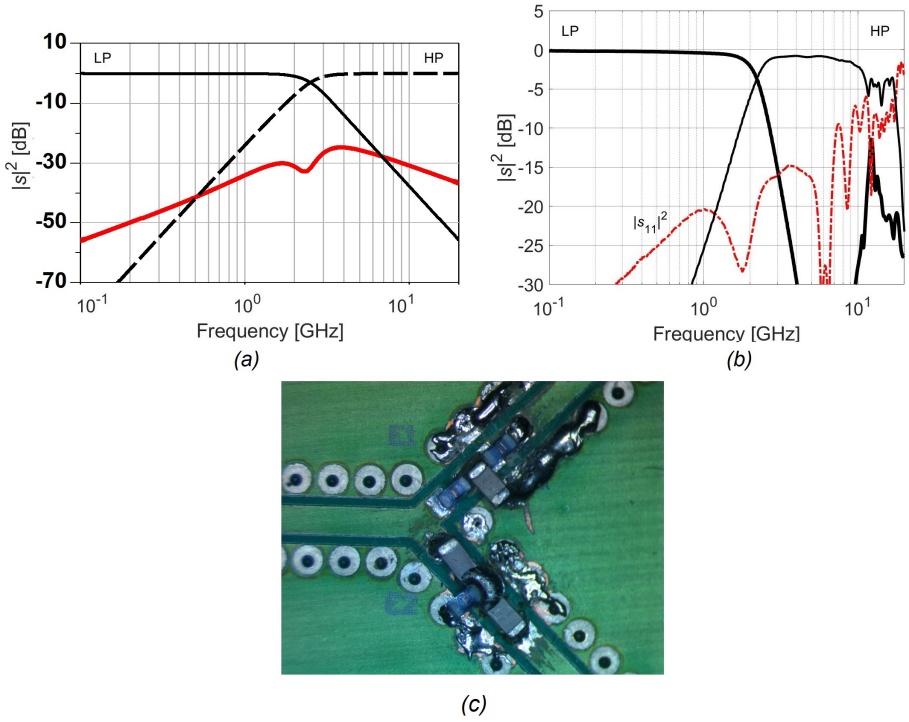


**Figure 2.13:** $(a)$ ADS simulation $(b)$ VNA measurements PCB filter sample for the third order 2.5 GHz complementary diplexer

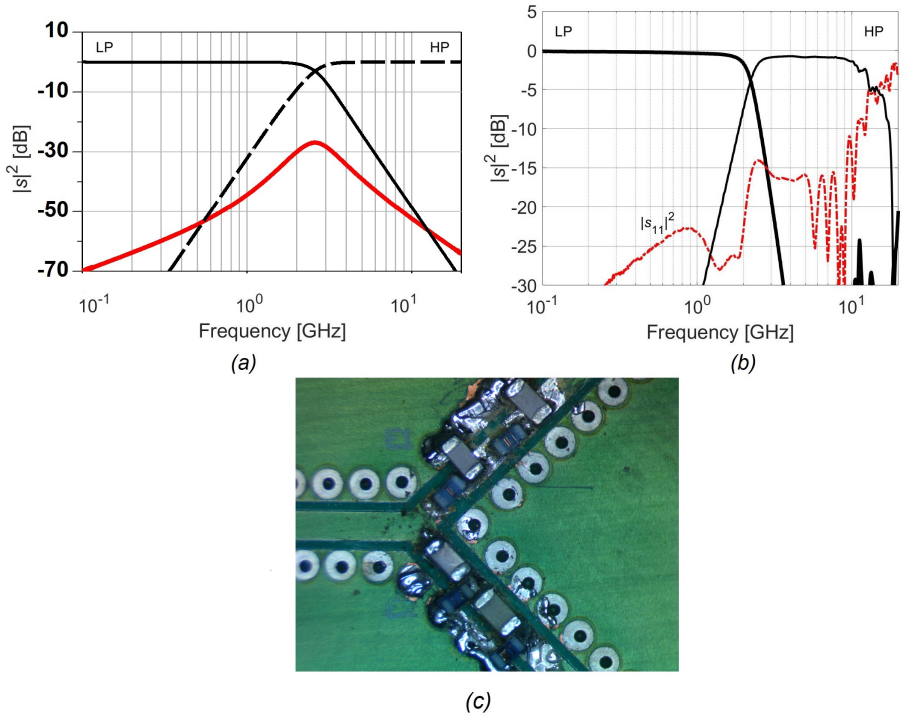


**Figure 2.14:** $(a)$ ADS simulation $(b)$ VNA measurements PCB filter sample for the fourth order 2.5 GHz complementary diplexer

**All of the four 2.5 GHz filters show similar performance with the 800 MHz ones however their $s_{11}$ is higher in value than the 800 MHz which was expected due to the higher operating frequency and the usage of lumped elements in the filter.**

**We consider -15dB reflection acceptable for use in our complementary filters on this cutoff frequency. Under this conditions the filters are usable up to 7-7.5GHz depending on the order. For that frequency $s_{11}$ is less than 15dB.**
**Hence, for fundamental frequencies up to 2.5 GHz these filters can be used to properly terminate at least the third harmonic.**

## 2.5. Filter design conclusion

The measurements were worse than the simulations, as one would expect, since in our simulations we did not include all of the parasitic elements, various delay lines and placement of the lumped elements on the PCB. However, even with all of those shortcomings, the filters are usable to terminate the SMPA up to the 10th harmonic for the 800 MHz filter and at least the third harmonic on the 2.5GHz filter. Therefore, we will proceed to show the benefits of using such filters on the output of an SMPA.

# 3. Drain efficiency of an SMPA terminated with a complementary filter

## 3.1. Introduction

This chapter covers the theory and application about the efficiency measurement that has been covered to validate the usage of complementary (constant-resistance) networks as opposed to standard low-pass filters used on the output of switch-mode amplifiers(SMPAs). We want to study and show the efficiency improvements of the usage of complementary filters in a diplexer topology. First we explain the theory of the efficiency of an RFPA terminated with a lossless low-pass filter (LLLP) and a lossless all-pass network (ALP). Then we proceed to conduct an experiment with an SMPA that is terminated with LLLP and ALP networks where we show our results.

## 3.2. Drain efficiency

We first define the drain efficiency of a FET device as

$$\eta_{drain} = \frac{P_{RF}}{P_{DC}} = \frac{P_{RF}}{V_{DC} \cdot I_{DC}} \tag{3.1}$$

where $P_{RF}$ denotes the power of the first(primary) harmonic dissipated on the load (after the filter).

In figure 3.1 we show an SMPA terminated with an lossless low-pass filter. The LLLP exhibits a frequency dependent complex reflection $\rho_L(\omega)$, which gets further noticeable on higher frequencies than $\omega_0$ (the filters 3 dB design parameter). A typical frequency characteristic of the lossless low-pass filter is illustrated in figure 3.2. For a lossless filter we have $|S_{21}|^2 + |S_{11}|^2 = 1$. The most important feature is

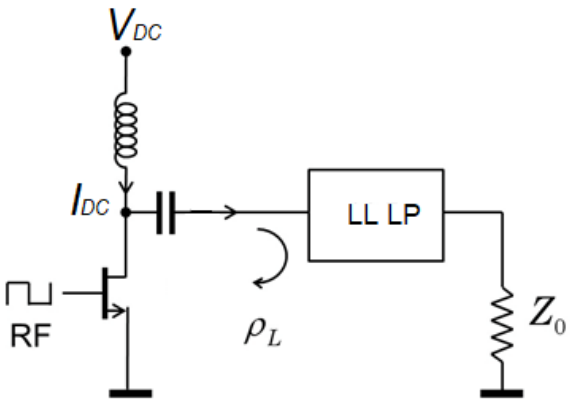


**Figure 3.1:** Lossless low-pass filter on the output of an SMPA

that in the stop-band ($\omega > \omega_0$) the filter reflects all of the power in the harmonics back to the PA.

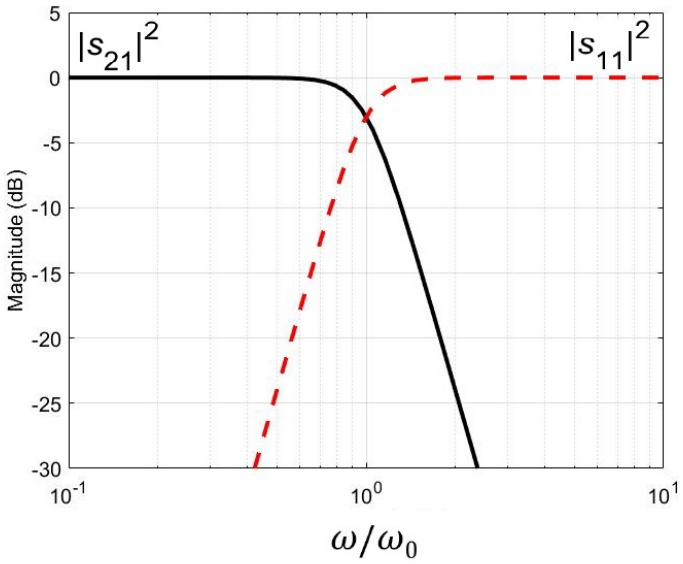


**Figure 3.2:** Lossless low-pass filter scattering parameters characteristic

Power balance requires that:

$$P_{DC} = P_{DIS}{}^{(1)} + P_{RF} \tag{3.2}$$

where $P_{DIS}^{(1)}$ counts all the dissipated power on the transistor. This includes all of the higher harmonics that reflect at the filter and went back to the transistor. The higher harmonics that get reflected from the filter dissipate on the amplifier increasing its temperature and hence lower the drain efficiency, note that the drain

efficiency depends on the FET channel conductance which directly depends on the carrier mobility which is temperature dependent: electron mobility reduces with temperature due to various forms of scattering. Manipulating equations 3.1 and 3.2 we can show that:

$$P_{DIS}^{(1)} = \frac{1 - \eta_{drain}}{\eta_{drain}} P_{RF} \tag{3.3}$$

Suppose we now terminate the SMPA with an absorbing low-pass (ALP) filter which passes any low frequency component, but absorbs all above the cutoff frequency as shown in figure 3.3, namely the power emitted by the PA in the stop-band is absorbed in the filter, rather than in the output of the transistor.

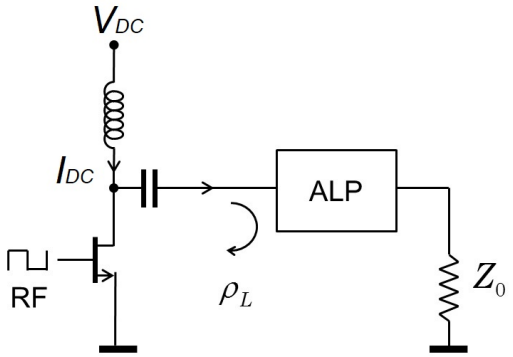


**Figure 3.3:** Lossless all-pass filter on the output of an SMPA

In this case the higher harmonics leave and never return back to the SMPA. The scattering parameter characteristic of the ALP is shown in figure 3.4[1].

The input impedance of such an ALP is always equal to $Z_0$ and there is no reflection present.

In this case, the power balance is given by:

$$P_{DC} = P_{DIS}^{(2)} + P_{ALP} + P_{RF} \tag{3.4}$$

Here we added the $P_{ALP}$ to represent power loss in the absorbing filter and which does not heat the transistor. Consequently $P_{DIS}^{(}2)$ should be smaller than $P_{DIS}^{(}1)$. We can estimate $P_{ALP}$ by considering that the SMPA emits a square wave. If we include all the harmonics above the first for a square wave signal with power $P_{SQ}$, the power in the first harmonic is $P_{RF} = \frac{8}{\pi^2} P_{SQ}$, where $P_{ALP} = (1 - \frac{8}{\pi^2}) P_{SQ}$.

[1]The red line is only here for illustration, ideally $|S_{11}|^2 = 0$

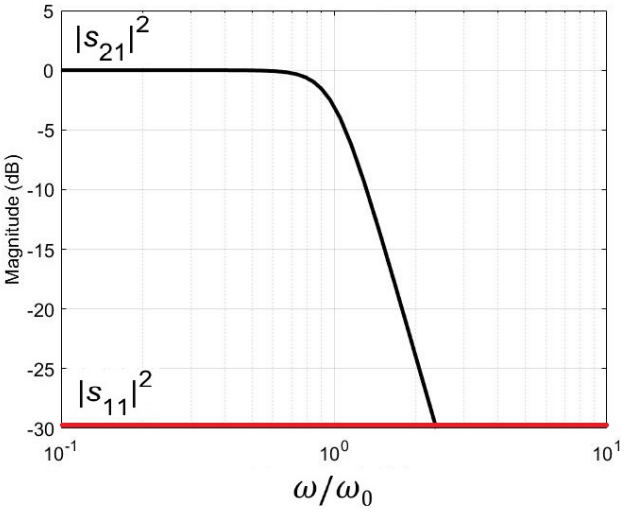


**Figure 3.4:** All-pass filter scattering parameters characteristic

Manipulating equation 3.4 and the above equations we can write:

$$P_{DIS}^{(2)} = \left(\frac{1}{\eta_{drain}} - \frac{\pi^2}{8}\right) P_{RF} \tag{3.5}$$

It may seem that $P_{DIS}^{(2)}$ may become negative if $\eta_{drain}$ becomes higher than $8/\pi^2$ however, that is not possible because $\eta_{drain}$ can never exceed $8/\pi^2$ for a square wave signal.

If we divide $P_{DIS}^{(2)}$ and $P_{DIS}^{(1)}$ we get a normalized graph of the improvement possible by absorbing the reflected harmonics shown on figure 3.5. Here it is clear that for a drain efficiency less than $8/\pi^2$ the complementary networks dissipate less power on the transistor. To illustrate this improvement in an example, suppose a drain efficiency of 0.6 and $P_{DIS}^{(1)}$ of 1 Watt for the LLLP termination. In that case for the ALP network termination yields $P_{DIS}^{(2)} \approx 0.65$W which means that using an ALP filter, in theory, yields less heating for $\approx 0.36$W which is $\approx$ 36% less than the LLLP for the given drain efficiency.

**Thus being said, a network configuration that dissipates the power of the higher harmonics on itself and not the amplifier will result in a higher drain efficiency as shown on figure 3.5**.

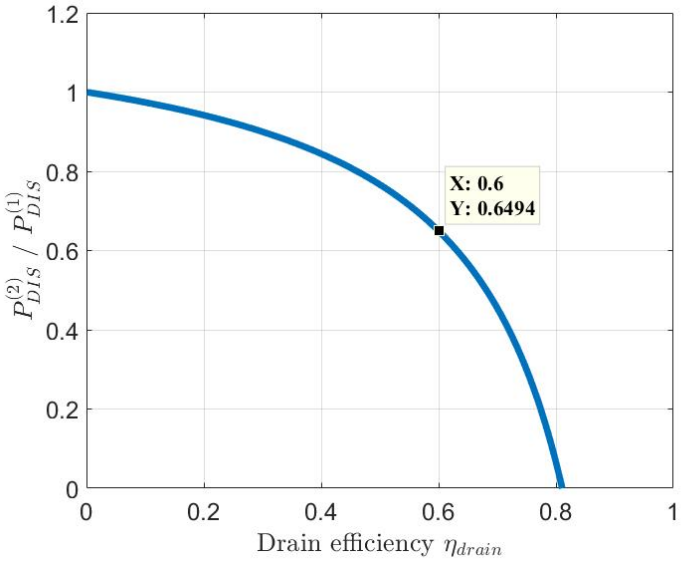


**Figure 3.5:** Lossless all-pass filter on the output of an SMPA

## 3.3. Experimental verification

To confirm the theory expectations that the dissipation on the FET is reduced when we terminate an SMPA with a complementary filter an experiment was conducted. We used a prototype switching power amplifier made by Eridan Communications, Inc., USA, which features a GaN field-effect transistor, an inductor and a DC-blocking capacitor at it's output. The amplifier is designed to operate as a switch in the frequency range between 50 MHz and 3 GHz. In this experiment, we are interested in our ability to alter the drain efficiency of this amplifier, hence the specifics of the amplifier design were outside the scope of this work. We used the differential clock output from a digital pattern generator to drive the switchmode amplifier. The amplifier output was not modulated in this experiment. The test setup is shown on figures 3.6 and 3.7.

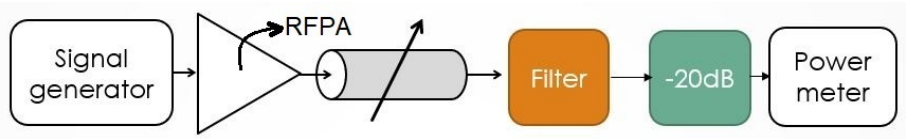


**Figure 3.6:** Filter termination experiment

On figure 3.6, on the output of the filter we get a 20 dB attenuated $P_{RF}$ measurement on the power meter, however, the higher harmonics that were reflected on the filter get back through the delay line to the SMPA.

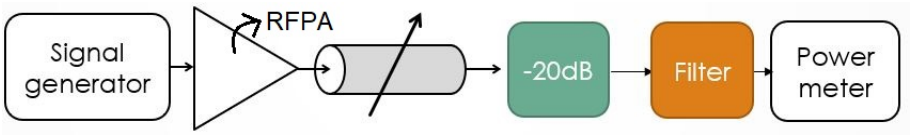


**Figure 3.7:** $Z_0$ termination experiment

If we use the configuration as on figure 3.7 we still get a 20 dB attenuated $P_{RF}$ on the power meter however due to the fact that the signal is beforehand attenuated 20dB and the reflection is further attenuated by 20 dB we can assume that the reflection $\rho_L$ is close to 0. Here, we have a $Z_0$ termination of the SMPA while on figure 3.6 we did not have the same case.

We first terminate the RFPA with a LLLP filter and an attenuator behind it. Then we switch the attenuator and filters positions in the chain. By using this approach we show that a lossless low-pass filter exhibits a lower drain efficiency $\eta_{drain}$ compared to a filter that has a $\rho_L \approx 0$ as shown in figure 3.7.

In addition to that comparison we show that in fact a complementary filter (CMP) exhibits a higher drain efficiency $\eta_{drain}$ and that the efficiency does not change with changing the position of the filter and attenuator in the measurement chain. Note that the reason we compare the measurement by comparing AT/LLLP and AT/CMP in the transmission is that we ensure that the filter insertion loss has no effect on the measurement. We do not compare the LLLP and CMP filters due to the fact that insertion loss is not the same.

Furthermore with changing the length of the variable delay line (VDL) we show that standard lossless low-pass filters vary in efficiency with the length of the VDL while $Z_0$ termination filters do not impact on the efficiency. We changed the VDL length to 3 positions depending on where the second harmonic is minimal, maximal and where the amplifier gives out maximum power on the output (as the 1st harmonic power). Ideally an SMPA should not have even order harmonics, however, this happens due to two reasons: (a) the SMPA acts like a time varying impedance so it modulates the odd order harmonics entering from the output, which produces the even mode harmonics, and, (b) the measurements were done on single ended inverse D class amplifier which furthermore produces even order harmonics. Adjusting to a minimal second harmonic, brings the SMPA output closest to ideal, desired output. The measurement setup is shown on figure 3.8.

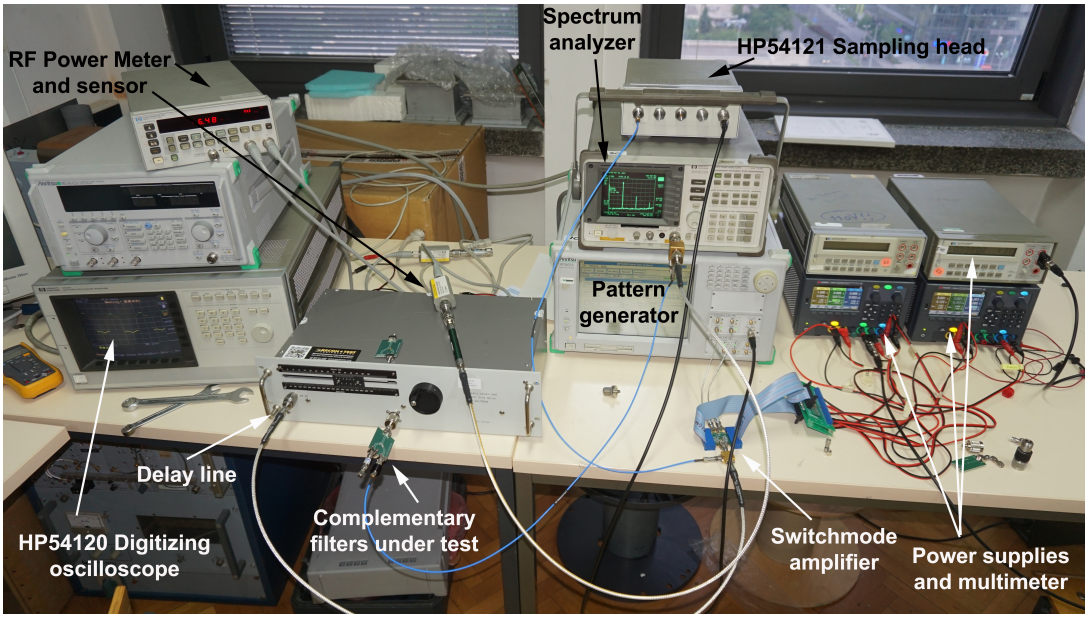


**Figure 3.8:** Measurement setup

## 3.4. Drain efficiency is greater when terminated /w complementary filter

We used the 800MHz 3dB point 4th order Butterworth filter and compared it to our complementary diplexer at the same frequency which was 540 MHz. Using the spectrum analyzer and VDL found a point where the 2nd harmonic is minimal (we used the measurement configuration on figure 3.7). At this frequency we measure the following parameters[2] as shown in table 3.1. Then we switch the positions of the filters and attenuators and measure again.

| Type | $P_{DC}[V]$ | $I_{DC}[mA]$ | $P_{RF}[dBm]$ | $\eta_{drain}$ |
|---|---|---|---|---|
| LP - Att | 4 | 96 | -6.27 | 30.81% |
| $Z_0$ - LP | 4 | 84 | -6.39 | 34.25% |
| CMP - Att | 4 | 80 | -6.49 | 35.06% |
| $Z_0$ - CMP | 4 | 84 | -6.50 | 35.3% |

**Table 3.1:** Measured parameters on 540 MHz

Using our digitizing oscilloscope we managed to capture the output of the amplifier. The capturing process is shown on figure 3.9. The process is repeated

[2]For computing the $\eta_{drain}$ we have to add +27 dB (20dB from the attenuator, 6 dB from the coupler and 1 dB from the band-pass filter for the extraction of the signal) on the table values of $P_{RF}$

for all of the filter and attenuator positions. On figure 3.10 we can compare

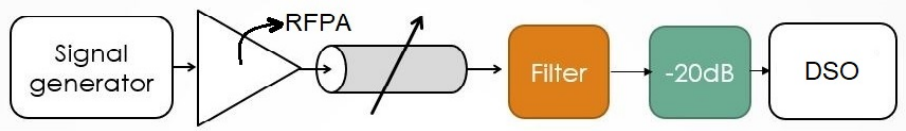


**Figure 3.9:** Output waveform capture with a digitizing signal oscilloscope (DSO)

the waveforms when the reflection $\rho_L$ is minimal (a), and (b) when we used a standard low-pass filter that rejects harmonics back to the amplifier. The result is that in figure (b) we lose the square property of the waveform while on figure (a) it still exists .

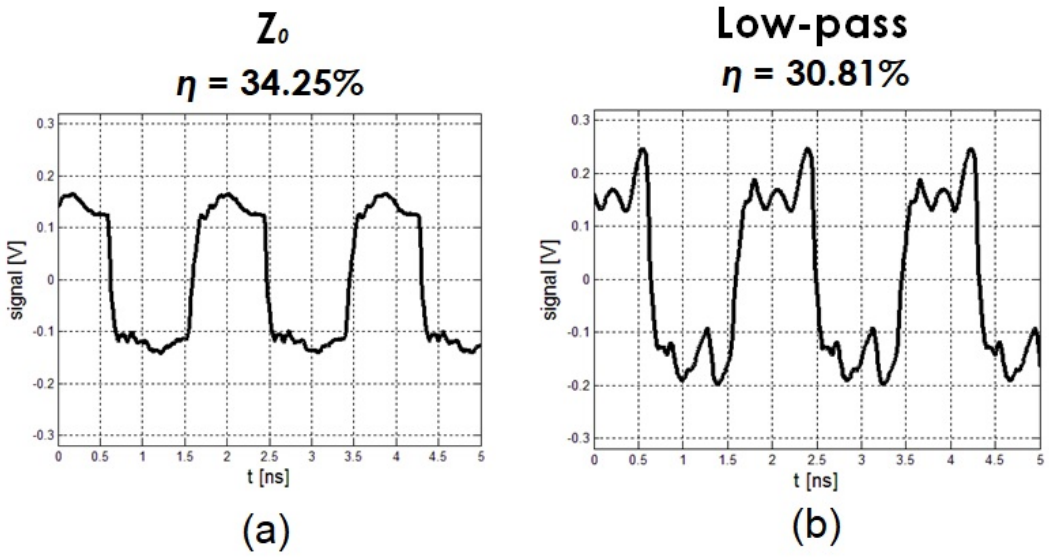


**Figure 3.10:** Output waveforms on 540 MHz for a loseless LP and input $Z_0$ loseless LP filter

As we can see from the table and from the figures there has been a rise in drain efficiency of $\approx 3\%$ removing the reflection property of the filter of the higher frequencies.

On the other hand we did the same procedure with a complementary Butterworth diplexer. The waveforms are shown on figure 3.11.

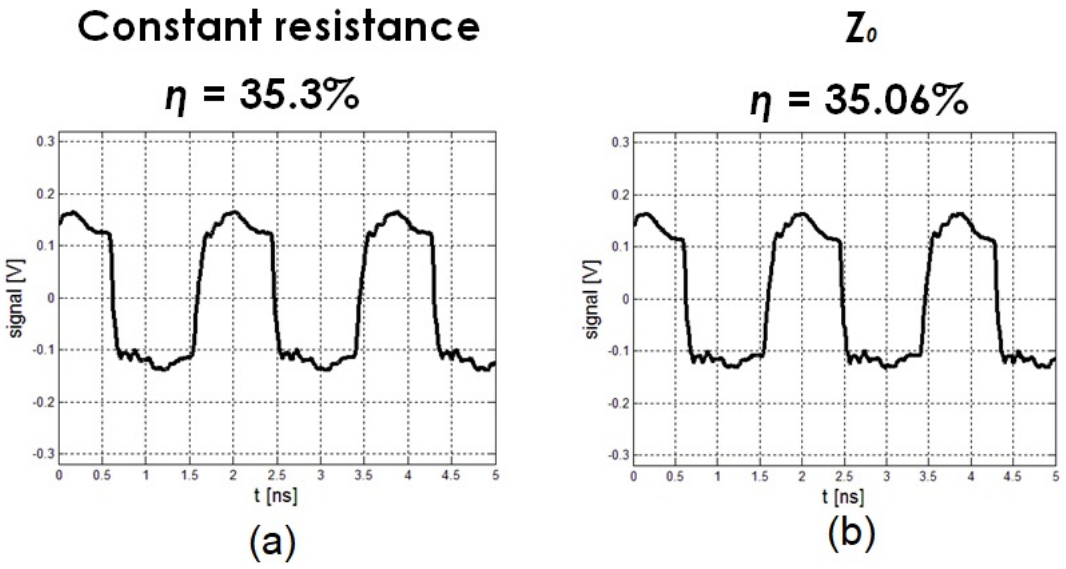


**Figure 3.11:** Output waveforms on 540 MHz for a lossless complementary diplexer and input $Z_0$ diplexer filter

As we can see from both the table and the figure, the efficiency for both of the measurements stays same, while the waveform keeps the square property, and the efficiency of the constant resistance filter is higher than both the low-pass and $Z_0$ input low-pass filter.

**We came to the conclusion that the usage of a complementary (constant resistance) filter results in a higher and consistent drain efficiency than using only a low-pass filter.**

## 3.5. Drain efficiency is more stable when terminated /w complementary filter

Stability of the drain efficiency means that the drain efficiency does not depend on the phase of filter reflection or the distance between the amplifier and the

harmonic filter. This in turn means that changes in carrier frequency also have little or no effect on the drain efficiency.

In the previous section we set the length of the VDL so that the power of the second harmonic is minimal. We noticed that with small variety in the VDL length we can actually measure more points so we chose to investigate what happens when we set the length so that the second harmonic is minimal, maximal and that the $P_{RF}$ is maximum. The filters we used here are the 2.5 GHz 3dB point low-pass and complementary diplexer which were designed earlier and the $f_0 = 1260$ MHz. The same experiment as in the previous section was conducted, with changing the position of the attenuator and filters. The results are shown in table 3.2.

| Type | Length | $P_{DC}[V]$ | $I_{DC}[mA]$ | $P_{RF}[dBm]$ | $\eta_{drain}$ |
|---|---|---|---|---|---|
| LP - Att | $l_{min} = 260°/GHz$ | 5 | 106 | -6.6 | 20.56% |
| | $l_{max} = 303°/GHz$ | | 118 | -6.5 | 18.98% |
| | $l_{RFmax} = 235°/GHz$ | | 131 | -5.9 | 19.5% |
| $Z_0$ - LP | $l_{min} = 260°/GHz$ | 5 | 110 | -6.5 | 20.41% |
| | $l_{max} = 303°/GHz$ | | 110 | -6.5 | 20.41% |
| | $l_{RFmax} = 235°/GHz$ | | 107 | -6.5 | 20.97% |
| CMP - Att | $l_{min} = l_{max} = l_{RFmax}$ | 5 | 113 | -6.28 | 20.88% |
| $Z_0$ - CMP | $l_{min} = l_{max} = l_{RFmax}$ | 5 | 110 | -6.45 | 20.63% |

**Table 3.2:** Measured parameters on 1260 MHz

For the low-pass filter in table 3.2 the drain efficiency $\eta_{drain}$ varies with the change of the length of the VDL. This means that, when we are using a low-pass filter on the output of a SMPA, the distance between the filter and the SMPA matters, meaning that the phase increases or decreases the performance of the circuit. Furthermore when we compare tthe $Z_0$ input measurements for the low-pass filter we get a more stable $\eta_{drain}$ with less variance in results. Now, when we look at the complementary filters results we show that for any of the 3 lengths of the VDL the drain efficiency stays the same with less variance. This means that the complementary networks, no matter the length of the VDL, are less phase sensitive.

On figures 3.12 and 3.13 we can see the signal waveform on the output of the amplifier. While figure 7 compares the low-pass and $Z_0$ input impedance we can

see that the latter presents a more consistent $\eta_{drain}$ than the single input low-pass filters while on 3.13 the waveforms look the same with a similar $\eta_{drain}$.

**The usage of the complementary filter shows that the drain efficiency stays constant and that the usage of such a filter presents a phase independency ie. it does not matter on what length we put the filter from the output of the SMPA, the efficiency stays the same since the phase is independent of the reflection.**

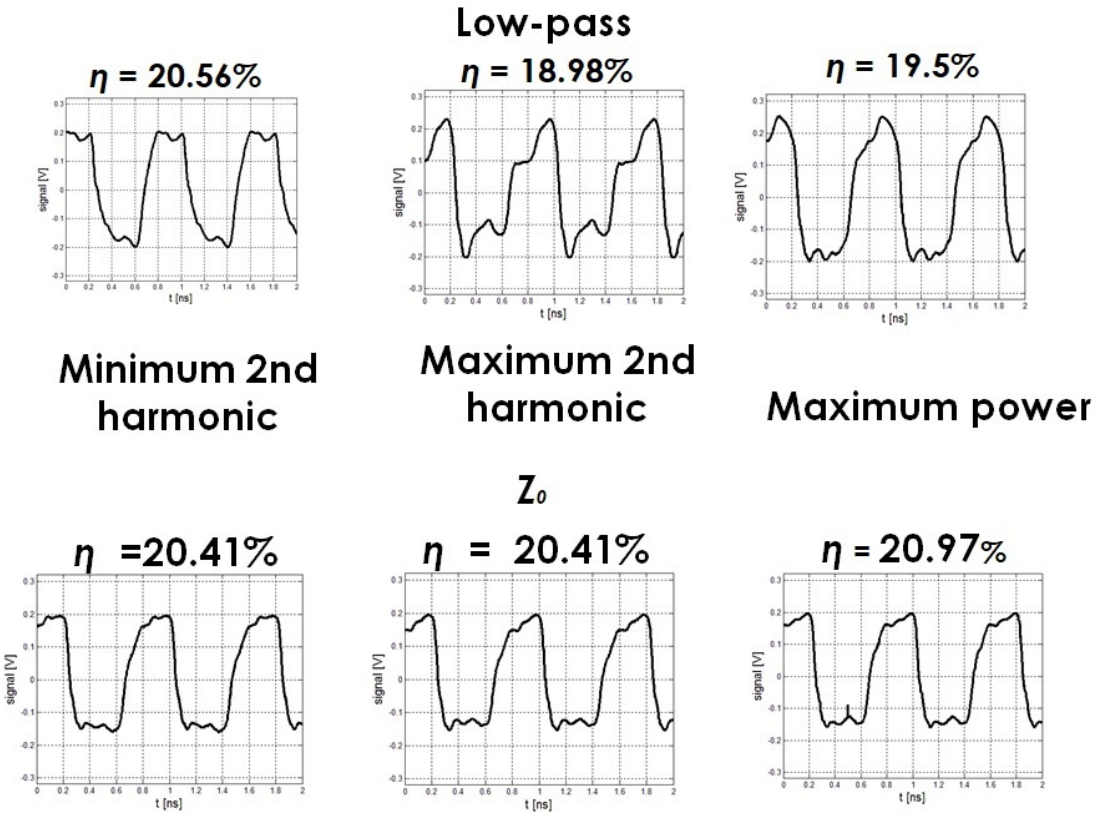


**Figure 3.12:** Output waveform on 1260 MHz for a LLLP and input $Z_0$ LLLP filter

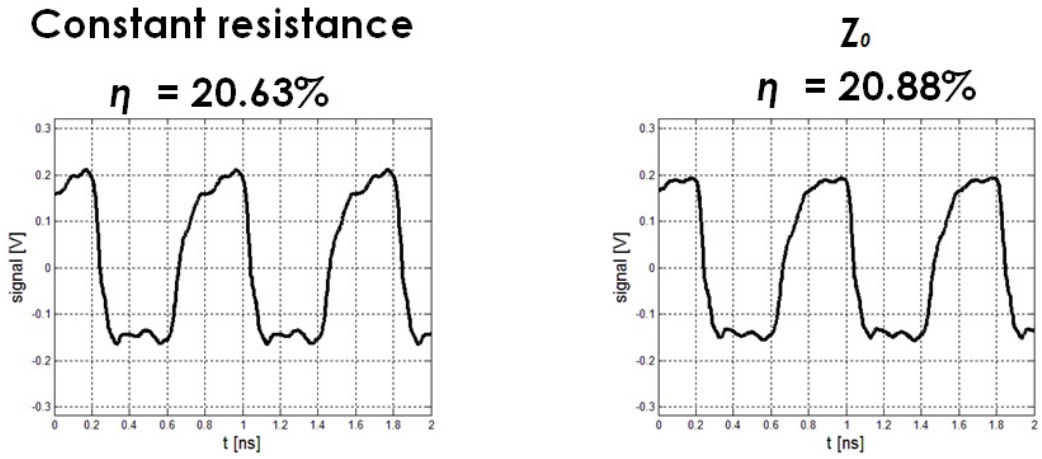


**Figure 3.13:** Output waveform on 1260 MHz for a lossless complementary diplexer and input $Z_0$ diplexer filter

## 3.6. Conclusions on drain efficiency

We showed that using complementary (constant resistance) filters results in higher and more consistent drain efficiency than using only a low-pass filter. Furthermore, we showed that using such a filter presents a phase independency. In other words, it does not matter on what length we put the filter from the output of the SMPA, the efficiency stays the same.

# 4. Time-domain reflectometry as a quality test

## 4.1. Introduction

This chapter covers the basics and application of time-domain reflectometry (TDR) that was used as a quality test for the complementary filters. Since the quality of the complementary filters is that that $|s_{11}|^2$ is small as possible we need to determine the main sources of any assembly problems that could arise and increase $|s_{11}|^2$. A MATLAB model was developed to simulate TDR response, which was then compared to the measurement in order to define the quality of the filter.

## 4.2. TDR fundamentals

Time domain reflectometry (TDR) is an impedance measurement [16] method that measures reflections on a transmission line in real time. The idea is to send a signal $f(t)$ along the line and from the character and delay of the reflection deduce the character and location of the discontinuity. A discontinuity that results in a reflection coefficient $\Gamma(f)$ at the measuring port will produce there a reflected signal $f_r(t)$ given by :

$$f_r(t) = \int_{-\infty}^{+\infty} \Gamma(f)F(f)e^{j2\pi ft}df \tag{4.1}$$

where $F(f)$ is the Fourier transform of the signal $f(t)$. Most commercial TDR systems today use a fast rise step ($\approx$ 100ps) function for the signal that travels along the transmission line [17]. Depending on the termination of the transmission line the discontinuities have unique waveforms. Such examples are presented on figures 4.1, 4.2, 4.3 and 4.4 [18] [16].

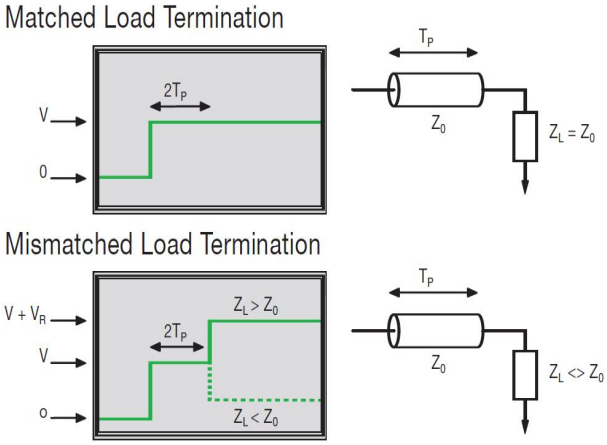


**Figure 4.1:** TDR response for various termination and discontinuities [18]

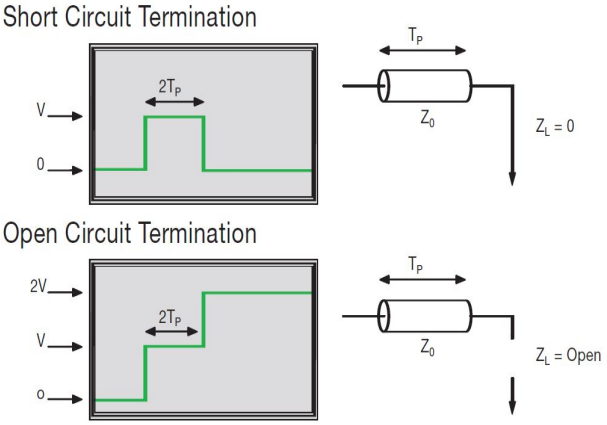


**Figure 4.2:** TDR response for various termination and discontinuities [18]

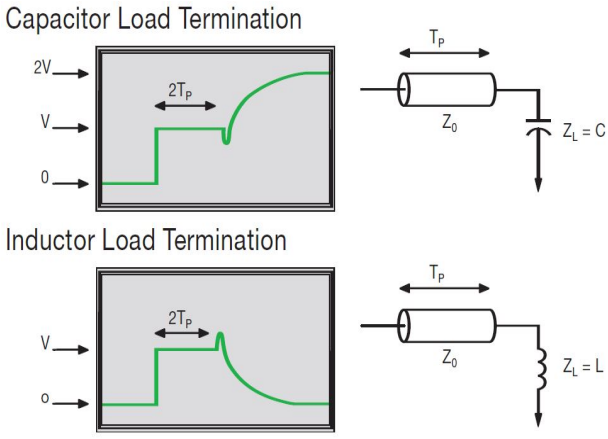


**Figure 4.3:** TDR response for various termination and discontinuities [18]

## 4.3. Measuring the filters

Using the waveforms shown in the prevoious figures we can determine the quality of the reflection and the elements that build the filters.The filter sections

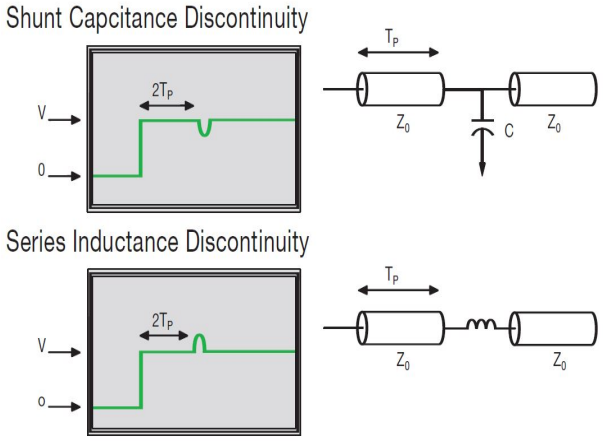


**Figure 4.4:** TDR response for various termination and discontinuities [18]

are shown on figure 4.5, (a) is the low-pass filter while (b) is the complementary filter.

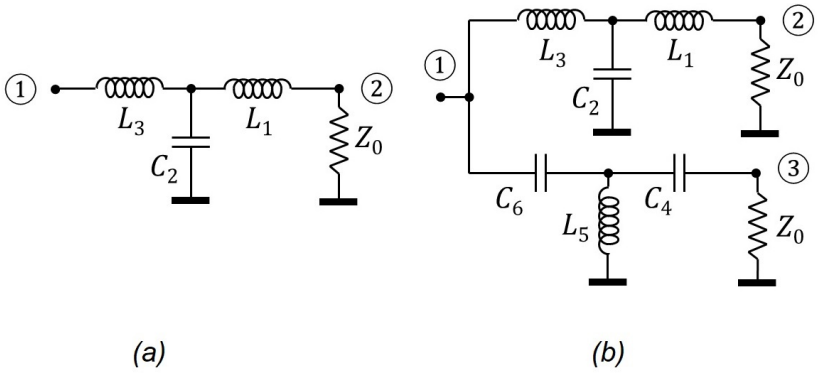


**Figure 4.5:** Schematic of the two tested filters

We compared the 4th order low-pass filter and an 4th order complementary filter in terms of their TDR response on figure 4.6 where (a) shows the TDR response of the LLLP filter while (b) presents the response of the complementary filter.

It is clear that the reflection from the complementary filter (b) looks almost the same as the matched termination on figure 4.1 however, even if it looks close to the match we can see two small shunt capacitance dips as on 4.4. We chose to further investigate the origin of these dips. [19]. On figure 4.7 (a) we show the comparison of all 4 order filters while on (b) we show a slightly modified version of one of the filters. When there is no filter present the two 50-ohm transmission lines branching off present a 25-ohm load at the branch point which results in a reflection coefficient magnitude equal to 1/3 (shown as the red line). The step

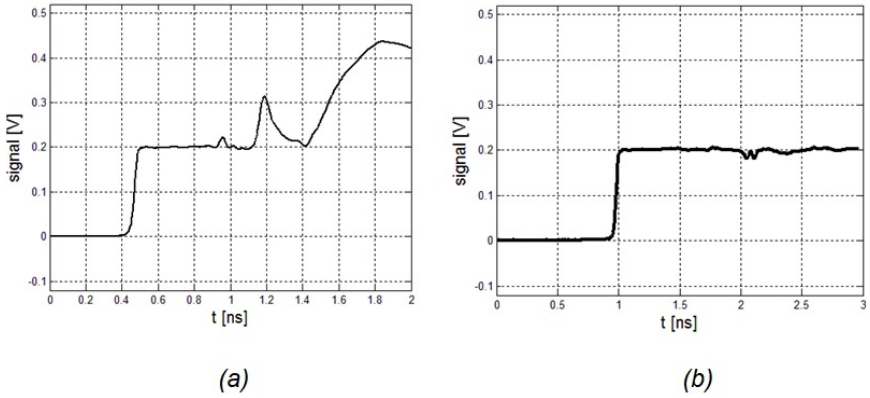


**Figure 4.6:** TDR waveforms of the LLLP and complementary filter

response hence dips below the 0.2 V horizontal level by a third of the step voltage as expected (0.2-V step is standard for TDR equipment).

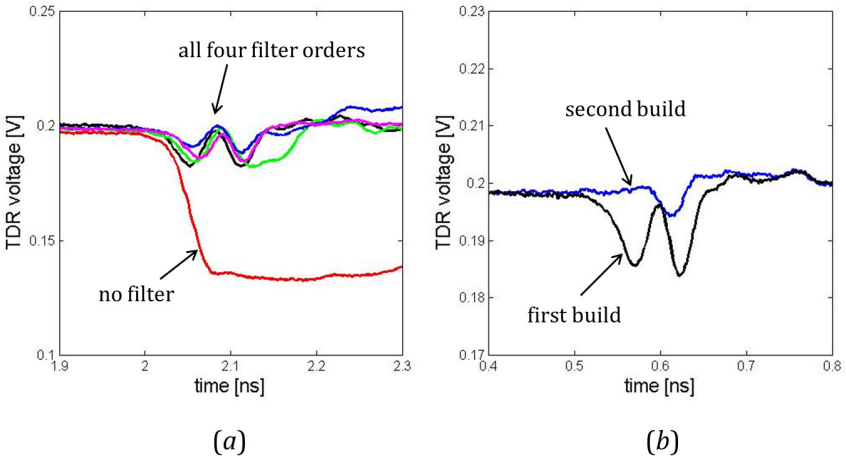


**Figure 4.7:** Closeup TDR waveforms complementary filter showing the *parasitic* discontinuities

On (a) we show that all four filters orders exhibit the same problem : *(i)* mismatch in the phase of the branches, and *(ii)* the resonances in the individual components. The mismatch *(i)* actually means that the elements in the one of parallel sections are not on the same electrical lengths as compared to the other section. To convince ourselves that the phase mismatch contributes to the increase of the input reflection, thus decreasing the complementary filters performance we rebuilt the the fourth order filter by moving the first inductor and capacitor of the two branches closer into the branching point. This resulted in an improvement in the response shown as the "second build" in figure 4.7 (b). This analysis illustrates an important note on the design and assembly of the

complementary filters : the phase of the input reflection on each of the filters and their difference is crucial for achieving low input reflection. Using ADS we simulated the delay lines in one of the branches of the filter which resulted in the following $s$ parameters show on figure 4.8. This further confirmed that

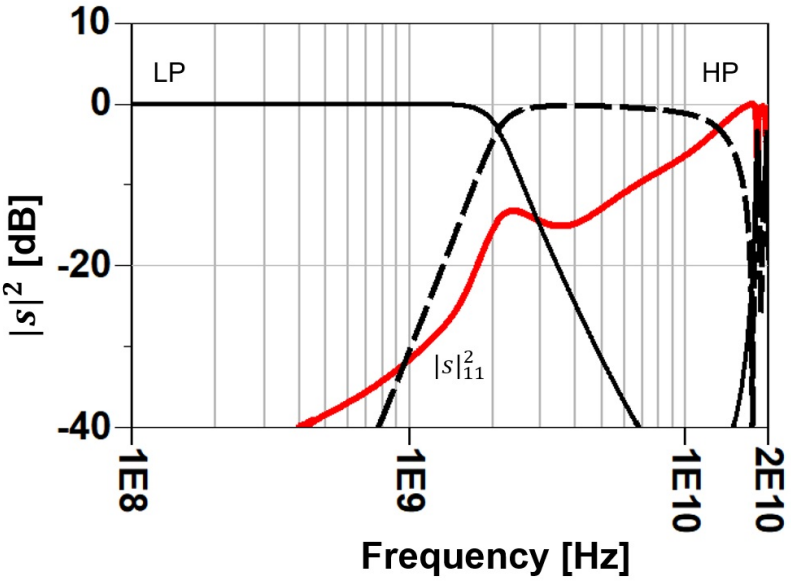


**Figure 4.8:** Complementary filter $s$ parameters with delay lines in one of the branches

building complementary filters presents a tighter constraint on the placement of the filter elements on the PCB since even a small mismatch or a delay line can further decrease the performance of the filters. The problem *(ii)* that consists of the resonances of individual components is negligible up to higher frequencies and solvable with smaller components (using 0402 instead 0603 or even smaller packages), however at some point we will be restricted with the power that passes through the filters (Doherty amplifiers emit up to several hundred watts of power [20], [21]) since smaller components have limited power ratings.

## 4.4. TDR simulation program using MATLAB

Using MATLAB by MathWorks we created a TDR simulation program. The flowchart for it is present on figure 4.9. First an ideal square wave is generated and then phase shifted so he starts from 0 and rises at T/2 thus producing an ideal TDR step generator with an infinitely short rise time. To make it look like a real TDR generator we present the Bessel-Thompson filtering in which the square wave exhibits real-time rise time. Once that is done we take the spectrum

of the square wave and multiply it with the spectrum of a generated reflection $\Gamma(\omega) = s_{11}(\omega)$ coefficient of the network we want to simulate. The resulting spectrum is actually the TDR spectrum and now we only have to use the inverse-Fourier transform to get the wanted TDR response in time domain. For example,

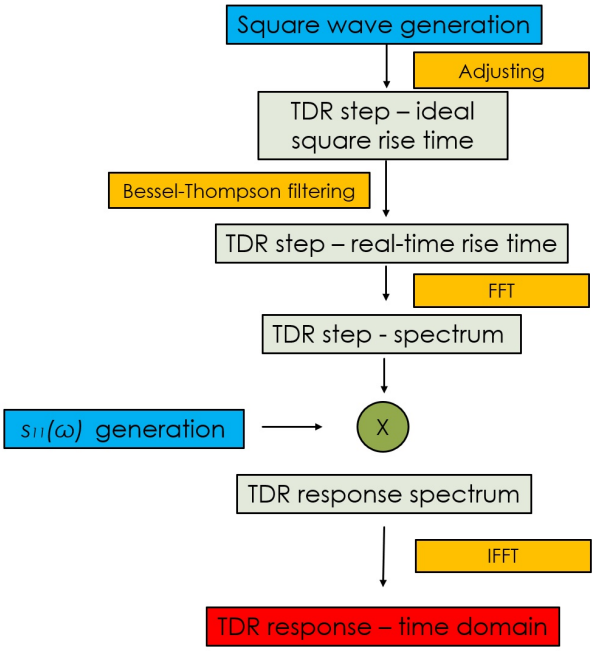


**Figure 4.9:** TDR program flowchart

using the program, we can simulate a TDR response for a network that consists of a series inductance discontinuity of $L = 1$ nH and $Z_0 = 50\ \Omega$. The TDR response is shown on figure 4.10. The simulation shows similarities with 4.4 where we can see a small upwards dip due to the inductance.

## 4.5. Simulation of the complementary filter TDR response

Using the MATLAB program introduced in the last section we chose to simulate the TDR response of the complementary filters in order to discover the values of the parasitic elements that can be seen as discontinuities at the transmission line. It is expected that the values from figure 4.7 (a) will be significantly small, around fF values. We show the results on figure 4.11.

The primary goal here was to discover the value of the capacitance discontinuity which ends up $C_{discontinuity} \approx 20$ fF. Since there are 2 dips on the measurements

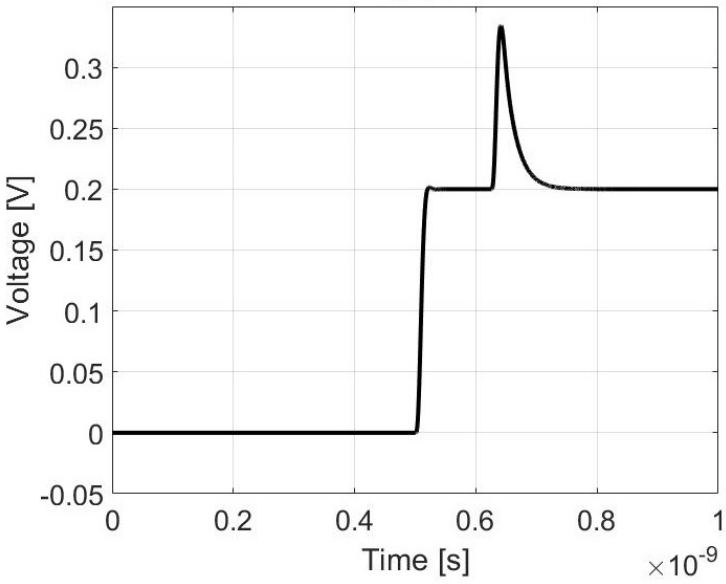


**Figure 4.10:** TDR simulation of a series inductor discontinuity network

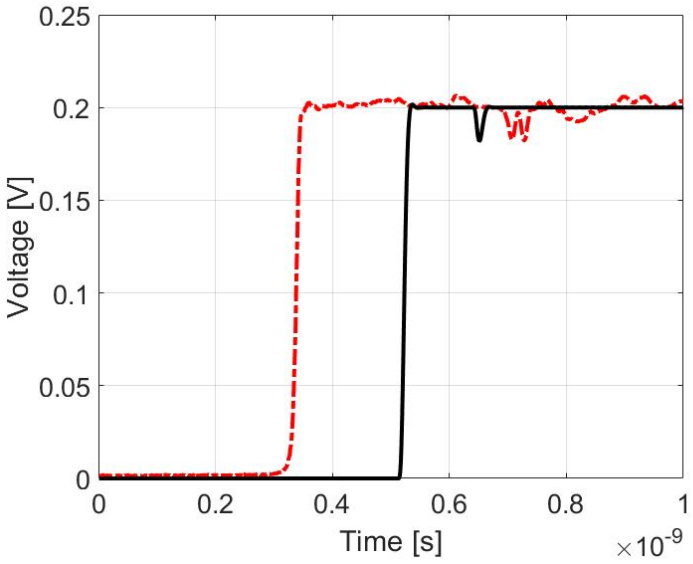


**Figure 4.11:** TDR simulation of the complementary filter response (black) and measured complementary filter response (red dashed)

we can conclude the measured filters reflection consists of two really close capacitive discontinuities of the same value. On our simulation there has been only one capacitive discontinuity implemented, however the value is roughly the same. Take a note that the time delay between the simulation and measurement is not relevant, the value of the discontinuity is only important.

## 4.6. TDR conclusion

Time domain reflectometry(TDR) presents a powerful tool for the quality characterization of complementary filters due to the fact that it is much more easier and intuitively to deduce the characters of the networks in the time domain than in the frequency domain with $s$ parameters on the VNA. Using the TDR we characterized the complementary filters and found out that they're losing performance due to the fact that the elements need to be placed much more precise than the elements in widely low-pass filters. The only way to increase the performance is to have tighter constraints in the assembly of such filters. Using a MATLAB program we managed to simulate the TDR behavior and approximated the value of the discontinuity in the complementary filters.

# 5. Conclusion

Constant resistance networks, and complementary filters in particular, has been introduced and validated for the use at the output of a radiofrequency switchmode amplifiers. We showed both in theory and measurements that using such networks increases and stabilizes the drain efficiency of the SMPA.

We have also found that the assembly of complementary filters presents a more stringent design and assembly tasks than lossless filters for this application due to the fact that the filter elements need to be placed very precisely so that the phases of the low-pass and high-pass sections match to realize the lowest $s_{11}$ parameter as possible.

We furthermore used time domain reflectometry (TDR) to evaluate the quality of the filters. Using TDR we managed to prove that the discontinuities happen due to the phase mismatch at the very input of the filters.

## 5.1. Acknowledgment

The author expresses his gratitude to Fran Kostelac for designing the printed circuit boards. The printed circuit boards were manufactured by Markovac d.o.o., Zagreb, while the filters were assembled and all of the experimental work has been performed at the Department of wireless communications (Zavod za radiokomunikacije) Faculty of electrical engineering and computing in Zagreb. This work has been funded in part under a contract between Faculty of Electrical Engineering and Computing in Zagreb and Eridan Communications, Inc. Santa Clara, CA, USA.

Equipment used:

- HP54120 Digitizing oscilloscope
- Rohde&Schwarz 40GHz VNA
- HP438/HP8485A Power meter and sensor
- WILTRON Variable Delay Line model 3114
- Anritsu MP1632A pattern generator (square-wave signal to drive the modulator)
- Keysight 36312A Programmable Power Supplies
- HP3478A multimeter
- HP3590B Spectrum Analyzer
- Demo unit of Eridan's switch-mode mixer modulator with GaN FET at the output stage

# Bibliography


[1] O. J. Zobel, "Theory and design of uniform and composite electric wave-filters," *The Bell System Technical Journal*, vol. 2, no. 1, pp. 1–46, Jan 1923.

[2] ——, "Distortion correction in electrical circuits with constant resistance recurrent networks," *The Bell System Technical Journal*, vol. 7, no. 3, pp. 438–534, July 1928.

[3] E. L. Norton, "Constant resistance networks with applications to filter groups," *The Bell System Technical Journal*, vol. 16, no. 2, pp. 178–193, April 1937.

[4] H. J. Carlin, "Gain-Bandwidth Limitations on Equalizers and Matching Networks," *Proceedings of the IRE*, vol. 42, no. 11, pp. 1676–1685, Nov 1954.

[5] K. S. Stull, "A Broadband Termination for IF Coaxial Lines," *Proceedings of the IRE*, vol. 49, pp. 365–366, January 1961.

[6] G. L. Matthaei, "Some Techniques for Network Synthesis," *Proceedings of the IRE*, vol. 42, no. 7, pp. 1126–1137, July 1954.

[7] G. R. Deily, "A constant-resistance band-pass filter," *Proceedings of the IEEE*, vol. 53, no. 3, pp. 328–329, March 1965.

[8] E. Zeheb and G. R. Deily, "On constant resistance networks," *Proceedings of the IEEE*, vol. 53, no. 8, pp. 1154–1155, Aug 1965.

[9] C. Y. Chang, "Constant resistance low-pass filter," *Proceedings of the IEEE*, vol. 54, no. 7, pp. 983–984, July 1966.

[10] J. D. Trudel, "Superior constant resistance common ground filter networks," *Proceedings of the IEEE*, vol. 58, no. 3, pp. 515–516, March 1970.

[11] M. E. V. Valkenburg, *Modern Network Synthesis.* John Wiley & Sons, 1964.

[12] M. A. Morgan, *Reflectionless Filters.* Artech House, 2017.

[13] "RO4000 Series, High Frequency Circuit Materials," Rogers Corporation. [Online]. Available: https://www.rogerscorp.com/documents/726/acs/RO4000-LaminatesData-Sheet.pdf

[14] "SMA Female End Launch Connector 292-04a-6," South West Microwave. [Online]. Available: https://mpd.southwestmicrowave.com/wp-content/uploads/2018/06/292-04A-6.pdf

[15] "Inductor products," American Technical Ceramics. [Online]. Available: http://www.atceramics.com/UserFiles/inductor_products.pdf

[16] P. Somlo and J.D.Hunter, *Microwave impedance measurement*, 1st ed. Peter Peregrinus LTD., London, UK, 1985.

[17] "CT100 Automated Metallic TDR," MOHR Test and Measurement LLC, Richland, WA 99354 USA . [Online]. Available: http://www.mohr-engineering.com/tdr-cable-tester-features-CT100.php

[18] "TDR Impedance Measurements: A Foundation for Signal Integrity," Tektronix. [Online]. Available: http://www.tek.com/dl/55W_14601_2.pdf

[19] A. Brizić and D. Babić, "Constant-resistance filters with diplexe architecture for S-band applications," in *2019 41th International Convention on Information and Communication Technology, Electronics and Microelectronics (MIPRO)*, May 2019.

[20] Walter Sneijers, "Doherty Architectures in UHF - White Paper," Ampleon, Nijmegen, Netherlands. [Online]. Available: https://www.ampleon.com/documents/white-paper/AMP-WP-2016-0826.pdf

[21] Fred Stefanik, "Doherty Amplifiers "101", and How They Apply to DTV," Hitachi Kokusai Electric Comark LLC. [Online]. Available: http://www.comarktv.com/wp-content/uploads/ABS16-01-stefanik.pdf

**Switch-mode radiofrequency amplifiers with complementary filters**


## Abstract

This work introduces a novel approach in using constant resistance networks, specially complementary filters in a diplexer configuration, on the output of a radio-frequency switch-mode modulator. Theory concepts and design for the filters, with a crossover frequency of 800 MHz and 2.5GHz, are considered and the filters were assembled and measured. Based on the measurements and simulations we concluded that switchmode RF power amplifiers terminated with complementary filters exhibit higher and more consistent drain efficiency than when terminated with only a low-pass filter. Despite increasing and stabilizing the drain efficiency, the filters present a slightly more stringent assembly procedure in comparison to the widely used low-pass filters due to the fact that the $s_{11}$ parameter, which we want to be minimal as possible, falls off due to phase mismatch between the low-pass and high-pass section. We used time domain reflectometry(TDR) to evaluate the quality of the filter's assembly. Using TDR simulations and measurements we identified the discontinuities that lower the performance of the complementary filters.



**Keywords:** Constant Resistance Networks, Complementary Filters, RF, RFPA, RF Power Amplifier, RFSMPA, Switch-mode Modulators, Analog Filter, Diplexer, Butterworth Characteristic, Drain Efficiency, Time Domain Reflectometry, TDR

**Preklopna radiofrekvencijska pojačala s komplementarnim filtrima**


**Sažetak**

Ovaj rad uvodi novi pristup pri korištenju konstantnih otporničkih mreža, pobliže komplementarnih filtara u konfiguraciji dipleksera, na izlazu radiofrekvencijskih preklopnih modulatora. Dana su teorijska razmatranja i dizajn filtara te mjerenja napravljenih filtara s karakterističnom frekvencijom na 800 MHz i 2.5 GHz. Zaljučeno je da preklopna pojačala zaključena s komplementarnim filtrima imaju veću i stabilniju efikasnost nego kada su zaključena samo s nisko-propusnim filtrom. Iako povećavaju korisnost, proizvodnja ovakvih filtara predstavlja kompliciraniji postupak naspram korištenih nisko-propusnih filtara, iz razloga što $s_{11}$ parametar, za koji želimo da bude što manji moguć, ovisi o faznom neslaganju između nisko-propusne i visoko-propusne sekcije, te u slučaju većeg neslaganja opada, pri čemu performanse filtra također opadaju. Kao kvalitativna metoda za evaluaciju filtara koristi se reflektometrija u vremenskoj domeni. Korištenjem simulacija i mjerenja putem reflektometrije potvrđeno je da diskontinuiteti nastaju zbog faznog neslaganja između dviju filtarskih sekcija te je aproksimiran ekvivalentni iznos diskontinuiteta.



**Ključne riječi:** Konstantne otporničke mreže, Komplementarni Filtri, RF, RFPA, RF Pojačala Snage, RFSMPA, Preklopni Modulator, Analogni Filtar, Diplekser, Butterworthova Karakteristika, Korisnost odvoda, Reflektometrija u vremenskoj domeni, TDR